ELSEVIER

Coastal Engineering 30 (1997) 125–156

COASTAL ENGINEERING

Boussinesq equations for wave transformation on porous beds

E.C. Cruz [a], M. Isobe [b], A. Watanabe [b]

[a] *Numerical Analysis Laboratory, Technical Research Institute, Toa Corporation, 1-3 Anzen-cho Tsurumi-ku, Yokohama 230, Japan*

[b] *Department of Civil Engineering, University of Tokyo, Hongo 7-3-1, Bonkyo-ku, Tokyo 113, Japan*

Abstract

A set of time-dependent vertically-integrated equations is derived to model the horizontally two-dimensional transformation of waves on a porous bed. The basic equations, called the Boussinesq equations for porous beds, contain the leading orders of nonlinearity and dispersivity. A general resistance equation has been used for the porous medium. The applicability bounds of the basic equations, limited by weak dispersivity and underestimated porous damping rates in deeper waters, have been extended by adding dispersion terms to the momentum equations and calibrating the resulting dispersion relation with a linear theory for porous beds. A numerical method based on finite differences is employed to solve the equations for two dimensions. The extended equations are verified for damped wave propagation on a horizontal bed, wave transformation on uniform porous slopes and combined refraction, diffraction, shoaling and damping around a submerged porous breakwater with an opening.

Keywords: Wave transformation; Boussinesq equations; Nonlinearity; Dispersivity; Porous bed; Damping

1. Introduction

There are numerous situations in the study of wave effects on the coastal environment in which one has to deal with a porous bathymetry. Among the many examples, the propagation of a broken wave on a permeable beach and wave transformation around artificial reefs and submerged porous structures are probably the most common. In order to understand the complex physical processes that occur in these enviroments, it is necessary to have a mathematical model that reproduces the basic properties of the wave field over a conceivable range of wave conditions.

PII S0378-3839(96)00039-7

Accurate computations of the wave field have become possible with the use of mathematical models of varying degrees of limitation on two important wave parameters: wave nonlinearity and dispersivity. Nonlinearity is a requisite for the generation of higher harmonics on regions of constricted depths, such as crowns of submerged structures, and dispersivity is necessary for wave celerity dependent on the wave frequency. A number of mathematical models to study the transformation of waves over impermeable beds have been proposed and verified. In subsequent developments, modelling of the wave field on porous beds has been done. Rojanakamthorn et al. (1990) derived an elliptic-type equation for permeable beds following the derivation of the mild-slope equation. This model is fundamentally limited by the use of linear theory. Although dispersivity is arbitrary, the absence of the nonlinear component and the invocation of the monochromatic wave concept are reasons for the inability to predict the decomposition of waves behind submerged breakwaters. Using a perturbation method, Isobe et al. (1991) and Cruz et al. (1992) derived a set of time-dependent nonlinear equations for one-dimensional transformation. Since these models include the leading order of nonlinearity, they are able to generate the higher harmonics on the shallow water regions. However, the inherent dispersivity is weak and, consequently, the frequency-dependent wave decomposition phenomenon beyond submerged breakwaters cannot be reproduced. Kioka et al. (1994) derived one-dimensional shallow water equations for porous structures. Although the free water depth is assumed arbitrary, the underlying solid bed was assumed horizontal, a basic limitation when simulating the combined shoaling and porous damping processes occurring, for instance, in submerged porous structures.

In this paper, we derive a set of Boussinesq equations over a porous bed of arbitrary thickness uderlain by a solid bottom at arbitrary depth in two horizontal dimensions after determining the governing equations and boundary conditions for the three-dimensional wave motion. The leading order of nonlinearity is incorporated. However, the weak dispersivity of Boussinesq-type equations is retained. This is corrected by adding dispersion terms to the basic momentum equations and matching the resulting dispersion relation with that of an appropriate theory. From this, a quantification of the applicability bounds of the new model can be made. This approach follows the idea used by Madsen et al. (1991) for impermeable beds. The fundamental properties of the model are clarified by results of numerical computations for uniform porous beds, which are compared with theory. Then the model is tested for wave transformation on plane porous slope and for simultaneous refraction, diffraction, reflection and porous damping around a submerged porous breakwater with an opening. Data obtained from physical model experiments are used to verify the numerical results.

2. Governing equations and boundary conditions of wave motion on porous beds

The variables and domain of interest are shown in Fig. 1. The free surface is displaced by $\eta(x,y,t)$ from still water. Free water has a thickness of $h(x,y)$ and the porous layer of thickness $h_s(x,y)$ is underlain by an impermeable bottom at $z=$

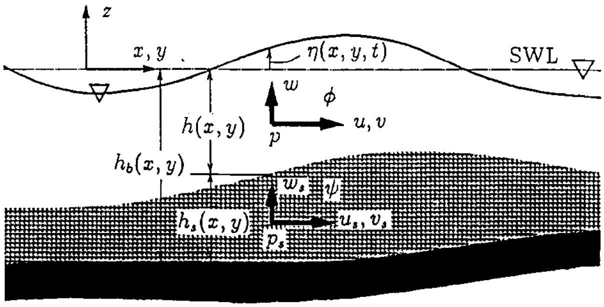

Fig. 1. Definition of variables.

$-h_b(x,y)$. The flow is assumed incompressible and irrotational in both layers. The equation of motion inside the porous medium is given by

$$\lambda \frac{\mathrm{d}\boldsymbol{U}_s}{\mathrm{d}t} + \frac{1}{\rho}\nabla_3(p_s + \rho g z) + F_r + F_i = 0 \tag{1}$$

where λ is the porosity, $\boldsymbol{U}_s \equiv (u_s, v_s, w_s)$ the seepage velocity vector, p_s the pore pressure, ρ the fluid density, g the gravity acceleration, $\nabla_3 \equiv (\partial/\partial x, \partial/\partial y, \partial/\partial z)$ the gradient operator, F_r the porous drag resistance term, F_i the inertial resistance term and $\mathrm{d}/\mathrm{d}t \equiv \partial/\partial t + \boldsymbol{U}_s \cdot \nabla_3$ denotes the total derivative. In steady flows, F_r just balances the drop in piezometric head along the flow direction. The head drop is related to velocity by the nonlinear resistance equation

$$F_r \equiv -\frac{1}{\rho}\nabla_3(p_s + \rho g z) = \alpha_1 \boldsymbol{U}\mathrm{s} + \alpha_2 |\boldsymbol{U}_s| \boldsymbol{U}_s \tag{2}$$

where α_1 and α_2 are coefficients which represent the laminar and turbulent flow resistances respectively. In general, these coefficients depend on the properties of the medium and the fluid. In unsteady flows, an inertial resistance term F_i is necessary to account for the divergence and convergence of streamlines in the presence of the solid surfaces. F_i is the product of the displaced fluid mass, the virtual mass coefficient and the local acceleration in the flow direction. Per unit volume of water, this is expressed as

$$F_i \equiv (1-\lambda)(1+c_m)\frac{\mathrm{d}\boldsymbol{U}_s}{\mathrm{d}t} \tag{3}$$

where c_m is the added mass coefficient. c_m can be evaluated for individual regular shapes but is generally unknown for randomly packed granular solids. After Eqs. (2) and (3) are substituted in Eq. (1), the equation of motion becomes

$$c_r \frac{\mathrm{d}\boldsymbol{U}_s}{\mathrm{d}t} + \frac{1}{\rho}\nabla_3(p_s + \rho g z) + \alpha_1 \boldsymbol{U}_s + \alpha_2 |\boldsymbol{U}_s| \boldsymbol{U}_s = 0 \tag{4}$$

where c_r is the inertial coefficient:

$$c_r \equiv \lambda + (1-\lambda)(1+c_m) \tag{5}$$

The mass conservation equation for the porous layer is

$$\nabla_3 \cdot (\lambda \boldsymbol{U}_s) = 0 \tag{6}$$

and since the porosity is assumed uniform, this gives

$$\nabla_3 \cdot \boldsymbol{U}_s = 0 \tag{7}$$

In the overlying free water, the usual equations of motion and mass conservation apply:

$$\frac{d\boldsymbol{U}}{dt} + \frac{1}{\rho}\nabla_3(p + \rho g z) = 0 \tag{8}$$

$$\nabla_3 \cdot \boldsymbol{U} = 0 \tag{9}$$

where $\boldsymbol{U} \equiv (u,v,w)$ is the water particle velocity, p the pressure and $d/dt = \partial/\partial t + \boldsymbol{U} \cdot \nabla_3$.

At the free surface, the dynamic and kinematic conditions are

$$p = 0 \quad z = \eta(x,y,t) \tag{10}$$

$$\frac{d}{dt}(z - \eta) \equiv w - \frac{\partial \eta}{\partial t} - \boldsymbol{u} \cdot \nabla \eta = 0 \quad z = \eta(x,y,t) \tag{11}$$

where $\nabla \equiv (\partial/\partial x, \partial/\partial y)$ is the horizontal gradient operator and $\boldsymbol{u} \equiv (u,v)$ the corresponding velocity vector. At the impermeable bottom, the normal velocity U_{sn} vanishes:

$$U_{sn} \equiv \boldsymbol{U}_s \cdot \boldsymbol{n}|\nabla_3(z + h_b)| \equiv \boldsymbol{U}_s \cdot \nabla_3(z + h_b) = \boldsymbol{u}_s \cdot \nabla h_b + w_s = 0 \quad z = -h_b(x,y) \tag{12}$$

where $\boldsymbol{n}$ is the unit normal vector and $\boldsymbol{u}_s \equiv (u_s, v_s)$ the horizontal seepage velocity. At the interface of the two layers, continuity of normal mass flux is prescribed. Across a unit bulk area, this is expressed as

$$(\rho \boldsymbol{U})_n = (\rho \lambda \boldsymbol{U}_s)_n \quad z = -h(x,y) \tag{13}$$

wherein the density in the respective layers cancels out because of the incompressibility assumption. Written in another way, this becomes

$$\boldsymbol{u} \cdot \nabla h + w = \lambda(\boldsymbol{u}_s \cdot \nabla h + w_s) \quad z = -h(x,y) \tag{14}$$

Finally, there must be equal pressures on both sides of the interface for it to exist:

$$p = p_s \quad z = -h(x,y) \tag{15}$$

The shear stress on the water-porous layer interface and porous layer–bottom interface will set-up boundary layers whose thicknesses may be comparable to the granule size. Sawaragi and Deguchi (1992), however, have shown that even for the highly nonlinear waves or for the highly porous media, the interface shear stress is small compared to the other terms in Eq. (1) or Eq. (4). The interface conditions (14) and (15) do not ensure the continuity of tangential velocities on both sides of the interface. We assume, therefore, that there is a boundary layer thick enough to equalize the tangential velocities yet thin enough not to affect the flows above or below it.

Eqs. (4), (7)–(9) describe the interior motions subject to boundary conditions (10), (11), (12), (14) and (15). In order to reduce the number of unknown variables, the following definitions of the velocity potentials Ψ and Φ are invoked:

$$U_s \equiv \nabla_3 \Psi \quad U \equiv \nabla_3 \Phi \tag{16}$$

With these, the continuity equations lead to the Laplace equations:

$$\nabla^2 \Psi + \Psi_{zz} = 0 \quad -h_b < z < -h \tag{17}$$

$$\nabla^2 \Phi + \Phi_{zz} = 0 \quad -h < z < \eta \tag{18}$$

where the subscripts denote partial differentiation. When Eq. (16) is used in Eqs. (4) and (8), the equations of motion can be expressed as follows:

$$c_r \left[\Psi_t + \frac{1}{2} (\nabla_3 \Psi)^2 \right] + \frac{p_s}{\rho} + gz + \alpha \Psi = 0 \tag{19}$$

$$\Phi_t + \frac{1}{2} (\nabla_3 \Phi)^2 + \frac{p}{\rho} + gz = 0 \tag{20}$$

With these, the boundary conditions involving the pressures can be expressed in terms of Ψ and Φ. The boundary conditions become

$$\Phi_t + \frac{1}{2} (\nabla_3 \Phi)^2 + g\eta = 0 \quad z = \eta \tag{21}$$

$$\Phi_z = \eta_t + \nabla \Phi \cdot \nabla \eta \quad z = \eta \tag{22}$$

$$\Psi_2 = -\nabla \Psi \cdot \nabla h_b \quad z = -h_b \tag{23}$$

$$\Phi_z + \nabla \Phi \cdot \nabla h = \lambda (\Psi_z + \nabla \Psi \cdot \nabla h) \quad z = -h \tag{24}$$

$$c_r \left[\Psi_t + \frac{1}{2} (\nabla_3 \Psi)^2 \right] + \alpha \Psi = \Phi_t + \frac{1}{2} (\nabla_3 \Phi)^2 \quad z = -h \tag{25}$$

The porous resistance coefficient α is defined as

$$\alpha \equiv \alpha_1 + \alpha_2 |U_s| \tag{26}$$

such that the porous resistance term in Eq. (19) can be temporarily linearized.

The problem is now governed by two linear equations constrained by five boundary conditions. The free-surface conditions and interface continuity of pressure are nonlinear in the new variables Ψ, Φ, and η. The problem itself is nonlinear since η is not known a priori.

3. Derivation of Boussinesq equations for porous beds

Wave motion is always characterized by three lengths: a water depth h_0, a wavelength l and a surface displacement amplitude a. To discern the relative importance of terms in the equations, we normalize the variables using the relevant characteristic length as follows:

$$x' \equiv \frac{x}{l} \quad y' \equiv \frac{y}{l} \tag{27}$$

$$z' \equiv \frac{z}{h_0} \quad h' \equiv \frac{h}{h_0} \quad h'_b \equiv \frac{h_b}{h_0} \quad \eta' \equiv \frac{\eta}{a} \tag{28}$$

$$t' \equiv \frac{t\sqrt{gh_0}}{l} \quad (\Psi',\Phi') \equiv \frac{(\Psi,\Phi)}{a\sqrt{gh_0}}\frac{l}{h_0} \tag{29}$$

The characteristic velocity is $\sqrt{gh_0}$ resulting in the characteristic time $l/\sqrt{gh_0}$ to travel a distance l. Likewise, from the definition of the potentials, the appropriate normalizer is $a\sqrt{gh_0}\,h_0/l$. If the above normalization is applied, the terms in the governing equations will group according to two nondimensional quantities, namely,

$$\varepsilon \equiv \frac{a}{h_0} \quad \mu \equiv \frac{h_0}{l} \tag{30}$$

These are respectively called the nonlinearity and dispersivity parameters. Omitting the primes for clarity, we can write the normalized equations as

$$\mu^2\nabla^2\Psi + \Psi_{zz} = 0 \quad -h_b < z < -h \tag{31}$$

$$\mu^2\nabla^2\Phi + \Phi_{zz} = 0 \quad -h < z < \eta \tag{32}$$

$$\mu^2(\Phi_t + \eta) + \varepsilon\frac{1}{2}\left[\mu^2\left(\Phi_x^2 + \Phi_y^2\right) + \Phi_z^2\right] = 0 \quad z = \varepsilon\eta \tag{33}$$

$$\mu^2(\eta_t + \varepsilon\nabla\Phi\cdot\nabla\eta) = \Phi_z \quad z = \varepsilon\eta \tag{34}$$

$$\Psi_z = -\mu^2\nabla\Psi\cdot\nabla h_b \quad z = -h_b \tag{35}$$

$$\Phi_z + \mu^2\nabla\Phi\cdot\nabla h = \lambda\left(\Psi_z + \mu^2\nabla\Psi\cdot\nabla h\right) \quad z = -h \tag{36}$$

$$\mu^2(c_r\Psi_t + \alpha\Psi) + \varepsilon\frac{1}{2}c_r\left[\mu^2\left(\Psi_x^2 + \Psi_y^2\right) + \Psi_z^2\right]$$
$$= \mu^2\Phi_t + \varepsilon\frac{1}{2}\left[\mu^2\left(\Phi_x^2 + \Phi_y^2\right) + \Phi_z^2\right] \quad z = -h \tag{37}$$

In these equations, we can see a distinction in the appearance of horizontal and vertical derivatives of the potentials. For example, terms containing derivatives in x and y are multiplied by μ^2 while those in z are not. This suggests that it is possible to decouple the horizontal and vertical dependencies by assuming a certain distribution in one plane and an arbitrary distribution in the other plane. Here, the potentials are assumed to admit arbitrary distributions $\psi(x,y,t)$, $\phi(x,y,t)$ in the horizontal direction and a power series expansion in the vertical direction as follows:

$$\Psi(x,y,z,t) = \sum_{n=0} [z + h_b(x,y)]^n \psi_n(x,y,t) \tag{38}$$

$$\Phi(x,y,z,t) = \sum_{n=0} [x + h(x,y)]^n \psi_n(x,y,t) \tag{39}$$

This expansion solution is a well-established method (Mei, 1989; Isobe and Kraus, 1983a,b).

The solutions are obtained by solving for $\psi_1, \psi_2 \ldots$ and then $\phi_1, \phi_2 \ldots$. First, by using the assumed potentials, the following expressions are obtained:

$$\nabla\psi = \sum_{n=0} (z + h_b)^n \nabla\psi_n + \sum_{n=0} (n+1)(z+h_b)^n (\nabla h_b)\psi_{n+1} \tag{40}$$

$$\begin{aligned}\nabla^2\psi = {} & \sum_{n=0} (z+h_b)^n \nabla^2\psi_n + \sum_{n=0} (z+h_b)^n \big[2(n+1)\nabla h_b \cdot \nabla\psi_{n+1} \\ & + (n+1)\nabla^2 h_b \psi_{n+1}\big] \\ & + \sum_{n=0} (z+h_b)^n (n+1)(n+2)(\nabla h_b)^2 \psi_{n+2}\end{aligned} \tag{41}$$

$$\sum_{n=0} (n+1)(z+h_b)^n \psi_{n+1} \tag{42}$$

$$\sum_{n=0} (n+1)(n+2)(z+h_b)^n \psi_{n+2} \tag{43}$$

Similar expressions are obtained for $\nabla\phi$, $\nabla^2\phi$, ϕ_z, ϕ_{zz}. Substituting Eqs. (41) and (43) into Eq. (31) results in

$$\begin{aligned}\sum_{n=0} (z+h_b)\big\{&(n+1)(n+2) r_b^2 \psi_{n+2} + (n+1)\mu^2\big[2\nabla h_b \cdot \nabla\psi_{n+1} + \nabla^2 h_b \psi_{n+1}\big] \\ & + \mu^2 \nabla^2 \psi_n\big\} = 0 \quad -h_b < z < -h\end{aligned} \tag{44}$$

$$r_b^2 \equiv 1 + \mu^2 (\nabla h_b)^2 \tag{45}$$

Since z is arbitrary, the coefficient of each power of $(z + h_b)$ must vanish, that is,

$$\begin{aligned}&(n+1)(n+2) r_b^2 \psi_{n+2} + (n+1)\mu^2\big[2\nabla h_b \cdot \nabla\psi_{n+1} + \nabla^2 h_b \psi_{n+1}\big] + \mu^2 \nabla^2 \psi_n = 0 \\ &n = 0,1,2,\ldots\end{aligned} \tag{46}$$

Eq. (46) is a recurrence relation for ψ_{n+2}. Substituting Eqs. (40) and (42) into the bottom boundary condition (35) gives

$$\sum_{n=0} (z+h_b)^n \big[(n+1) r_b^2 \psi_{n+1} + \mu^2 \nabla h_b \cdot \nabla\psi_n\big] = 0 \quad z = -h_b \tag{47}$$

or, when written in full,

$$\left[r_b^2\psi_1+\mu^2\nabla h_b\cdot\nabla\psi_0\right]+(z+h_b)^1\left[2r_b^2\psi_2+\mu^2\nabla h_b\cdot\nabla\psi_1\right]$$
$$+(z+h_b)^2\left[3r_b^2\psi_3+\mu^2\nabla h_b\cdot\nabla\psi_2\right]+\ldots=0\quad z=-h_b \tag{48}$$

Since the terms after the first are all zeroes, the result is

$$\psi_1=-\frac{\mu^2\nabla h_b\cdot\nabla\psi_0}{r_b^2} \tag{49}$$

There are two important implications of Eq. (49). First, by virtue of the recurrence relation (46), all odd-numbered ψ's appear only when the bottom changes, i.e., the even-numbered ψ's govern the propagation of waves of permanent form. Second, because r_b^2 appears whenever Eq. (46) is used, the effect of ∇h_b will geometrically decrease with n greater than 2. With ψ_1 determined and ψ_0 a free parameter, succeeding ψ's are obtained sequentially through Eq. (46). We show these up to $O(\mu^4)$:

$$\psi_2=-\frac{\mu^2}{2}\nabla^2\psi_0+\frac{\mu^4}{2}\nabla\cdot(\nabla h_b\nabla h_b\cdot\nabla\psi_0)+O(\mu^6) \tag{50}$$

$$\psi_3=\frac{\mu^4}{6}\left[2\nabla h_b\cdot\nabla(\nabla^2\psi_0)+\nabla^2h_b\nabla^2\psi_0+\nabla^2(\nabla h_b\cdot\nabla\psi_0)\right]+O(\mu^6) \tag{51}$$

$$\psi_4=\frac{\mu^4}{24}\nabla^2\nabla^2\psi_0+O(\mu^6) \tag{52}$$

$$\psi_5=O(\mu_6) \tag{53}$$

Boussinesq theory assumes that

$$O(\varepsilon)=O(\mu^2)<1 \tag{54}$$

implying that only the leading orders of nonlinearity and dispersivity need to be retained in ϕ and ψ. There is more practicality in this assumption since the next-order terms in Eqs. (50)–(53) contain the operator ∇ to, at least, fourth degree eventually requiring a fourth-degree velocity operator, a procedure that is computationally inefficient. Hence, we truncate the ψ's at $O(\mu^4)$, leading to

$$\Psi=\psi_0-\frac{\mu^2}{2}\left[2(z+h_b)\nabla h_b\cdot\nabla\psi_0+(z+h_b)^2\nabla^2\psi_0\right]+O(\mu^4) \tag{55}$$

which shows that only the three leading terms in Eq. (38) were included. It must be noted, however, that no assumption on the order of the bottom gradient is necessary even up to $O(\mu^4)$. Only when terms of $O(\mu^6)$ are included does an implicit mild-slope assumption need to be invoked to simplify the resulting equations.

Since Φ and Ψ are related through the interface boundary conditions, we can obtain Φ by applying either Eq. (36) or Eq. (37). We opted to use Eq. (36) because of its simpler form. To the same order, this is written

$$\sum_{n=0} (z+h)^n\left[(n+1)\left(1+(\mu\nabla h)^2\right)\phi_{n+1} + \mu^2\nabla h\cdot\nabla\phi_n\right]$$
$$= -\mu^2\lambda\nabla\cdot(h_s\nabla\psi_0) + O(\mu^4) \quad z=-h \tag{56}$$

which gives the solution

$$\phi_1 = -\frac{\mu^2\left[\nabla h\cdot\nabla\phi_0 + \nabla\cdot(h_s\nabla\psi_0)\right]}{1+(\mu\nabla h)^2} \tag{57}$$

Using Eq. (32), the following recurrence relation for ϕ_{n+2} can be obtained:

$$(n+1)(n+2)\phi_{n+2} + (n+1)\mu^2\left[2\nabla h\cdot\nabla\phi_{n+1} + \nabla^2 h\phi_{n+1}\right] + \mu^2\nabla^2\phi_n = 0$$
$$n=0,1,2,\ldots \tag{58}$$

Using this, we get the final form of Φ:

$$\Phi = \phi_0 - \frac{\mu^2}{2}\left\{2(z+h)\left[\nabla h\cdot\nabla\phi_0 + \lambda\nabla\cdot(h_s\nabla\psi_0)\right] + (z+h)^2\nabla^2\phi_0\right\} + O(\mu^4) \tag{59}$$

Just as in Ψ, only the first three terms in Eq. (39) are included.

The velocities in each layer can be obtained by applying the three remaining boundary conditions, namely, the nonlinear equations. First, the momentum equation in the water layer is obtained by applying the dynamic free-surface condition. Eq. (33) is first evaluated at $z=\varepsilon\eta$, then ∇ is applied to the resulting equation to get rid of ϕ_0:

$$\boldsymbol{u}_{0t} + \varepsilon\boldsymbol{u}_0\cdot\nabla\boldsymbol{u}_0 + \nabla\eta - \frac{\mu^2}{2}\nabla\left[h^2\nabla\cdot\boldsymbol{u}_{0t} + 2h\nabla h\cdot\boldsymbol{u}_{0t} + \lambda h\nabla(h_s\cdot\boldsymbol{u}_{s0t})\right]$$
$$= O(\varepsilon\mu^2,\mu^4) \tag{60}$$

where the velocities are

$$\boldsymbol{u}_0 \equiv \nabla\phi_0 \quad \boldsymbol{u}_{s0} \equiv \nabla\psi_0 \tag{61}$$

The momentum equation for the porous layer is obtained by applying the interface continuity of pressure. Eq. (37) is evaluated at $z=-h$ and ∇ is applied to the resulting equation to get rid of ψ_0:

$$c_r(\boldsymbol{u}_{s0t} + \varepsilon\boldsymbol{u}_{s0}\cdot\nabla\boldsymbol{u}_{s0}) + \nabla\eta + \alpha\boldsymbol{u}_{s0} - \frac{\mu^2}{2}\nabla\left[c_r\left(2h_s\nabla h_b\cdot\boldsymbol{u}_{s0t} + h_s^2\nabla\cdot\boldsymbol{u}_{s0t}\right)\right.$$
$$\left. + \alpha\left(2h_s\nabla h_b\cdot\boldsymbol{u}_{s0} + h_s^2\nabla\boldsymbol{u}_{s0}\right) + h^2\nabla\cdot\boldsymbol{u}_{0t} + 2h\nabla h\cdot\boldsymbol{u}_{0t} + 2\lambda\nabla\cdot(h_s\boldsymbol{u}_{s0t})\right]$$
$$= O(\varepsilon\mu^2,\mu^4) \tag{62}$$

The velocity variables defined by Eq. (61) are defined at the bottom. Other velocities, such as those at the interface or at the surface, may be taken as well. The choice of variable is arbitrary. However, different velocity variables lead to different dispersion relations (Madsen et al., 1991). In the case of porous beds, the choice of the velocity variable influences the porous damping property of the resulting equations. Here, we use the depth-averaged velocities, defined as

$$\overline{\boldsymbol{u}} \equiv \frac{1}{h+\varepsilon\eta}\int_{-h}^{\varepsilon\eta}\nabla\phi \mathrm{d}z \tag{63}$$

$$\overline{\boldsymbol{u}_\mathrm{s}} \equiv \frac{1}{h_\mathrm{b}-h}\int_{-h_\mathrm{b}}^{-h}\nabla\psi \mathrm{d}z \tag{64}$$

for two reasons: first, they lead to a compact vertically-integrated continuity equation; second, they are easily identified when prescribing the boundary conditions in a general horizontal two-dimensional computation. Eqs. (55) and (59) are substituted in Eqs. (63) and (64). The resulting equations can be recast as follows:

$$\boldsymbol{u}_0 = \overline{\boldsymbol{u}} + \frac{\mu^2}{2}\left[\frac{h^2}{3}\nabla(\nabla\cdot\overline{\boldsymbol{u}}) + h\nabla(\nabla h\cdot\overline{\boldsymbol{u}}) + h\nabla h\nabla\cdot\overline{\boldsymbol{u}} + 2\nabla h\nabla h\cdot\overline{\boldsymbol{u}}\right]$$
$$+\frac{\mu^2}{2}\lambda\left\{h\nabla\left[\nabla\cdot\left(h_\mathrm{s}\overline{\boldsymbol{u}_\mathrm{s}}\right)\right] + 2\nabla h\nabla\cdot\left(h_\mathrm{s}\overline{\boldsymbol{u}_\mathrm{s}}\right)\right\} + O(\mu^4) \tag{65}$$

$$\boldsymbol{u}_{\mathrm{s}0} = \overline{\boldsymbol{u}_\mathrm{s}} + \frac{\mu^2}{2}\left[\frac{h_\mathrm{s}^2}{3}\nabla(\nabla\cdot\overline{\boldsymbol{u}_\mathrm{s}}) + h_\mathrm{s}\nabla(\nabla h_\mathrm{b}\cdot\overline{\boldsymbol{u}_\mathrm{s}}) + h_\mathrm{s}\nabla h_\mathrm{b}\nabla\cdot\overline{\boldsymbol{u}_\mathrm{s}} + 2\nabla h_\mathrm{b}\nabla h_\mathrm{b}\cdot\overline{\boldsymbol{u}_\mathrm{s}}\right]$$
$$+O(\mu^4) \tag{66}$$

When Eqs. (65) and (66) are substituted into Eqs. (60) and (62), the following equations result:

$$\overline{\boldsymbol{u}}_\mathrm{t} + \varepsilon\overline{\boldsymbol{u}}\cdot\nabla\overline{\boldsymbol{u}} + \nabla\eta + \frac{\mu^2}{2}\left\{\frac{h^2}{3}\nabla(\nabla\cdot\overline{\boldsymbol{u}}_\mathrm{t}) - h\nabla\left[\nabla\cdot\left(h\overline{\boldsymbol{u}}_\mathrm{t}\right)\right] - \lambda h\nabla\left[\nabla\cdot\left(h_\mathrm{s}\overline{\boldsymbol{u}}_\mathrm{st}\right)\right]\right\}$$
$$= O(\varepsilon\mu^2, \mu^4) \tag{67}$$

$$c_\mathrm{r}\left(\overline{\boldsymbol{u}}_\mathrm{st} + \varepsilon\overline{\boldsymbol{u}_\mathrm{s}}\cdot\nabla\overline{\boldsymbol{u}_\mathrm{s}}\right) + \nabla\eta + \alpha\overline{\boldsymbol{u}_\mathrm{s}} + \frac{\mu^2}{2}\left(c_\mathrm{r}\frac{\partial}{\partial t} + \alpha\right)$$
$$\left[-\frac{2}{3}h_\mathrm{s}^2\nabla(\nabla\cdot\overline{\boldsymbol{u}_\mathrm{s}}) - h_\mathrm{s}\nabla(\nabla h_\mathrm{b}\cdot\overline{\boldsymbol{u}_\mathrm{s}}) + h_\mathrm{s}\nabla(h-h_\mathrm{s})\nabla\cdot\overline{\boldsymbol{u}_\mathrm{s}} + 2\nabla h\nabla h_\mathrm{b}\cdot\overline{\boldsymbol{u}_\mathrm{s}}\right]$$
$$-\frac{\mu^2}{2}\nabla\left[\nabla\cdot\left(h^2\overline{\boldsymbol{u}}_\mathrm{t}\right) + 2\lambda h\nabla\cdot\left(h_\mathrm{s}\overline{\boldsymbol{u}_\mathrm{s}}\right)\right] = O(\varepsilon\mu^2, \mu^4)$$

The continuity equation is obtained by substituting Eq. (59) into the kinematic free-surface condition (34) and recasting the potentials in terms of velocities:

$$\eta_\mathrm{t} + \nabla\cdot\left[(h+\varepsilon\eta)\overline{\boldsymbol{u}}\right] + \lambda\nabla\cdot\left(h_\mathrm{s}\overline{\boldsymbol{u}_\mathrm{s}}\right) = 0 \tag{69}$$

Unlike the momentum equations, the continuity equation is exact when formulated in terms of $\overline{\boldsymbol{u}}$, $\overline{\boldsymbol{u}_s}$. A more elaborate equation with truncation error would have been obtained if $\boldsymbol{u}_0$, $\boldsymbol{u}_{s0}$ were used instead.

Eqs. (67)–(69) comprise the set of Boussinesq equations for porous beds in nondimensional form.

3.1. Degenerate cases

For very long waves such as tides and seiches, μ^2 approaches zero and ε is $O(1)$. Then, in physical variables, Eqs. (67)–(69) reduce to

$$\eta_t + \nabla \cdot \left[(h+\eta)\overline{\boldsymbol{u}}\right] + \lambda \nabla \cdot \left(h_s \overline{\boldsymbol{u}_s}\right) = 0 \tag{70}$$

$$\overline{\boldsymbol{u}} + \overline{\boldsymbol{u}} \cdot \nabla \overline{\boldsymbol{u}} + g \nabla \eta = O(\mu^2, \varepsilon\mu^2, \mu^4) \tag{71}$$

$$c_r\left(\overline{\boldsymbol{u}_{st}} + \overline{\boldsymbol{u}_s} \cdot \nabla \overline{\boldsymbol{u}_s}\right) + g \nabla \eta + \alpha \overline{\boldsymbol{u}_s} = O(\mu^2, \varepsilon\mu^2, \mu^4) \tag{72}$$

These are referred to as the nonlinear long wave equations for porous beds.

In the absence of the porous layer, Eqs. (69) and (67) become, in physical variables,

$$\eta_t + \nabla \cdot \left[(h+\eta)\overline{\boldsymbol{u}}\right] = 0 \tag{73}$$

$$\overline{\boldsymbol{u}} + \overline{\boldsymbol{u}} \cdot \nabla \overline{\boldsymbol{u}} + g \nabla \eta + \frac{h}{2}\left\{\frac{h}{3}\nabla(\nabla \cdot \overline{\boldsymbol{u}}_t) - \nabla\left[\nabla \cdot (h\overline{\boldsymbol{u}}_t)\right]\right\} = O(\varepsilon\mu^2, \mu^4) \tag{74}$$

which are the Boussinesq equations derived by Peregrine (1967) for impermeable beds.

4. Extension to deeper waters

The dispersivity parameter is extremely important when modelling frequency-dependent phenomena such as wave propagation in deep water, wave grouping, irregular wave transformation and wave decomposition. The new equations retain the weak dispersivity of Boussinesq-type equations and, hence, cannot be used in deep water. A number of approaches have been successful in circumventing this inherent limitation in the case of impermeable beds. For example, Witting (1984) used a Pade approximation of the exact linear dispersion relation and matched it with the model dispersion relation based on the Taylor series expansion of the velocity at the free-surface. Madsen et al. (1991) added to the momentum equations higher-order terms that vanish in shallow water. By fitting with the linear dispersion relation up to the deep water limit, the optimum value of the coefficient of the additional terms was determined. Nwogu (1993) derived an alternate form of Boussinesq equations using a perturbation approach with the velocity at an arbitrary depth as the velocity variable. The vertical location of the velocity is determined such that the corresponding linear dispersion relation is a Pade approximation of the same order as that obtained by Madsen et al. (1991). In these approaches, the dispersion relation of the model equations is forced to comply with the dispersion relation of linear theory, which is exact for infinitesimal waves of arbitrary dispersivity.

4.1. Extended equations

In the current paper, we follow the idea used by Madsen et al. (1991) for impermeable beds. There are three important things to consider when applying this idea to porous beds. First, there are two fitting factors to obtain, one for each momentum equation. Second, dispersivity and porous damping are coupled properties so that these factors must be determined jointly. Third, there are two additional parameters introduced: the relative porous thickness h_s/h and a parameter to describe the property of the porous medium.

We rewrite Eq. (67) in physical variables, expanding the second dispersion term:

$$\bar{\boldsymbol{u}}_t + \bar{\boldsymbol{u}}\cdot\nabla\bar{\boldsymbol{u}} + g\nabla\eta - \frac{h^2}{3}\nabla(\nabla\cdot\bar{\boldsymbol{u}}_t) - \frac{h}{2}\nabla h\nabla\cdot\bar{u}_t - \frac{h}{2}\nabla(\nabla h\cdot\bar{\boldsymbol{u}}_t)$$
$$-\lambda\frac{h}{2}\left[\nabla\cdot\left(h_s\bar{\boldsymbol{u}}_{st}\right)\right] = 0 \tag{75}$$

The lowest-order momentum equation is

$$\bar{\boldsymbol{u}}_t + g\nabla\eta = O(\varepsilon,\mu^2,\dots) \tag{76}$$

Using this, the dispersion terms containing $\bar{\boldsymbol{u}}$ are approximated as follows:

$$h^2\nabla\left[\nabla\cdot\bar{\boldsymbol{u}}_t\right] \approx h^2\nabla\left[\nabla\cdot(-g\nabla\eta)\right] \tag{77}$$

$$h\nabla h\nabla\cdot\bar{\boldsymbol{u}}_t \approx h\nabla h\nabla\cdot(-g\nabla\eta)] \tag{78}$$

$$h\nabla\left[\nabla h\cdot\bar{\boldsymbol{u}}_t\right] \approx h\nabla\left[-\nabla h\cdot\nabla\eta\right] \tag{79}$$

Then we obtain the "zero equations" by multiplying Eqs. (77)–(79) by the same small factor, say $-\gamma$, and replacing the approximation by an equality:

$$-\gamma\left[h^2\nabla(\nabla\cdot\bar{\boldsymbol{u}}_t) + gh^2\nabla(\nabla^2\eta)\right] = 0 \tag{80}$$

$$-\gamma\left[h\nabla h\nabla\cdot\bar{\boldsymbol{u}}_t + gh\nabla h\nabla^2\eta\right] = 0 \tag{81}$$

$$-\gamma\left[h\nabla h\cdot\bar{\boldsymbol{u}}_t + gh\nabla[\nabla h\cdot\nabla\eta)\right] = 0 \tag{82}$$

These zero equations can then be added to Eq. (75) without changing either its meaning or truncation order:

$$\bar{\boldsymbol{u}}_t + \bar{\boldsymbol{u}}\cdot\nabla\bar{\boldsymbol{u}} + g\nabla\eta$$
$$-\left[\left(\frac{1}{3}+\gamma\right)h^2\nabla(\nabla\cdot\bar{\boldsymbol{u}}_t) + \left(\frac{1}{2}+\gamma\right)h\nabla h\nabla\cdot\bar{\boldsymbol{u}}_t + \left(\frac{1}{2}+\gamma\right)h\nabla(\nabla h\cdot\bar{\boldsymbol{u}}_t)\right]$$
$$-\gamma\left[gh^2\nabla(\nabla^2\eta) + gh\nabla h\nabla^2\eta + gh\nabla(\nabla h\cdot\nabla\eta)\right] - \frac{\lambda}{2}h\nabla\left[\nabla\cdot\left(h_s\bar{\boldsymbol{u}}_{st}\right)\right] = 0 \tag{83}$$

This can be simplified to the form of the original equation:

$$\bar{\boldsymbol{u}}_t + \bar{\boldsymbol{u}} \cdot \nabla \bar{\boldsymbol{u}} + g \nabla \eta + \frac{h^2}{6} \nabla(\nabla \cdot \bar{\boldsymbol{u}}_t) - \left(\frac{1}{2} + \gamma\right) h \nabla[\nabla \cdot (h \bar{\boldsymbol{u}}_t)] - \gamma g h \nabla[\nabla \cdot (h \nabla \eta)] - \frac{\lambda}{2} h \nabla[\nabla \cdot (h_s \bar{\boldsymbol{u}}_{st})] = 0 \tag{84}$$

Eq. (84) apparently indicates that only the second dispersion term in Eq. (67) has been corrected. However, Eq. (83) reveals that all dispersion terms are, in fact, considered. We could have included the factors 1/6 and 1/2 in Eqs. (80)–(82) but this would simply add terms to the resulting extended equation with a resulting different value of γ. For the porous layer, the lowest-order momentum equation is

$$c_r \bar{\boldsymbol{u}}_{st} + g \nabla \eta + \alpha \bar{\boldsymbol{u}}_s = O(\varepsilon, \mu^2, \dots) \tag{85}$$

Of the four bracketed dispersion terms in Eq. (68), we select only the last for extension:

$$\lambda \nabla[h \nabla \cdot (h_s \bar{\boldsymbol{u}}_s] \approx \lambda \nabla \left\{ -h \nabla \cdot \left[\frac{h_s}{c_r} (\alpha \bar{\boldsymbol{u}}_s + g \nabla \eta) \right] \right\} \tag{86}$$

The zero equation is obtained by multiplying by a small number, say $-\beta$:

$$-\lambda \beta \left\{ \nabla[h \nabla \cdot (h_s \bar{\boldsymbol{u}}_s)] + \frac{\alpha}{c_r} \nabla[h \nabla \cdot (h_s \bar{\boldsymbol{u}}_s)] + \frac{g}{c_r} \nabla[h \nabla \cdot (h_s \nabla \eta)] \right\} = 0 \tag{87}$$

When this is added to Eq. (68), the result in physical variables is

$$c_r(\bar{\boldsymbol{u}}_{st} + \bar{\boldsymbol{u}}_s \cdot \nabla \bar{\boldsymbol{u}}_s) + g \nabla \eta + \alpha \bar{\boldsymbol{u}}_s + \frac{1}{2}\left(c_r \frac{\partial}{\partial t} + \alpha\right) \times \left[-\frac{2}{3} h_s^2 \nabla(\nabla \cdot \bar{\boldsymbol{u}}_s) - h_s \nabla(\nabla h_b \cdot \bar{\boldsymbol{u}}_s) + h_s \nabla(h - h_s) \nabla \cdot \bar{\boldsymbol{u}}_s + 2 \nabla h \nabla h_b \cdot \bar{\boldsymbol{u}}_s \right] - \frac{1}{2} \nabla[\nabla \cdot (h^2 \bar{\boldsymbol{u}}_t)] - (1+\beta) \lambda \nabla[h \nabla \cdot (h_s \bar{\boldsymbol{u}}_s)] - \frac{\beta g}{c_r} \lambda \nabla[h \nabla \cdot (h_s \nabla \eta)] - \frac{\beta \alpha}{c_r} \lambda \nabla[h \nabla \cdot (h_s \bar{\boldsymbol{u}}_s)] = 0 \tag{88}$$

Eqs. (84) and (88) are the extended momentum equations which, together with Eq. (70), comprise the extended Boussinesq equations for porous beds.

4.2. Applicability bounds of the new Boussinesq equations

We extract the dispersion relation embedded in Eqs. (70), (84) and (88) for a horizontal bottom overlain by a uniform porous layer using the conventional one-dimensional Fourier analysis. The linearized equations are

$$\eta_t + h \bar{u}_x + \lambda h_s \bar{u}_{sx} = 0 \tag{89}$$

$$\bar{u}_t + g \eta_x - \left(\frac{1}{3} + \gamma\right) h^2 \bar{u}_{txx} - \gamma g h^2 \eta_{xxx} - \frac{1}{2} \lambda h h_s \bar{u}_{stxx} = 0 \tag{90}$$

$$c_r\overline{u}_{st} + g\eta_x + \alpha\overline{u}_s - \frac{1}{3}c_r h_s^2\overline{u}_{stxx} - \frac{1}{3}\alpha h_s^2\overline{u}_{sxx} - \frac{1}{2}h^2\overline{u}_{txx} - (1+\beta)\lambda h h_s\overline{u}_{stxx}$$
$$-\frac{\beta g}{c_r}\lambda h h_s\eta_{xxx} - \frac{\beta\alpha}{c_r}\lambda h h_s\overline{u}_{sxx} = 0 \tag{91}$$

A linear wave over porous bed is described by

$$(\eta, \overline{u}, \overline{u}_s) = (a_0, \overline{U}, \overline{U}_s)e^{i(kx-\omega t)} \tag{92}$$

where ω is the angular frequency, k the complex wave number, and a_o, $\overline{U}$, and $\overline{U}_s$ are the relevant amplitudes. Substitution into Eqs. (89)–(91) leads to

$$\begin{bmatrix} -\omega\left[1+\left(\frac{1}{3}+\gamma\right)k^2h^2\right] & -\frac{1}{2}\lambda\omega k^2 h h_s & gk(1+\lambda k^2h^2) \\ -\frac{1}{2}\omega k^2h^2 & -\omega\varphi & gk\left(1+\frac{\beta}{c_r}\lambda k^2 h h_s\right) \\ kh & \lambda k h_s & -\omega \end{bmatrix}\begin{bmatrix}\overline{U}\\ \overline{U}_s\\ a_0\end{bmatrix} = \begin{bmatrix}0\\0\\0\end{bmatrix} \tag{93}$$

where

$$\varphi \equiv \left(c_r + i\frac{\alpha}{\omega}\right)\left(1+\frac{1}{3}k^2h_s^2\right) + \lambda k^2 h h_s\left(1+\beta+i\frac{\beta\alpha}{\omega c_r}\right) \tag{94}$$

The solution is nontrivial only if the determinant of the coefficient matrix vanishes, leading to

$$\frac{\omega^2}{k^2gh}\left[1+\left(\frac{1}{3}+\gamma\right)k^2h^2\right]$$
$$= (1+\gamma k^2h^2) + \frac{\lambda h_s}{\varphi h}\left[1+\left(\frac{1}{3}+\gamma\right)k^2h^2\right]\left[1+\frac{\beta}{c_r}\lambda k^2 h h_s\right]$$
$$-\frac{\lambda k^2 h h_s}{2\varphi}\left[\left(1+\frac{\beta}{c_r}\lambda k^2 h h_s\right) - \frac{\omega^2 h}{g} + (1+\gamma k^2h^2)\right] \tag{95}$$

This is the linear dispersion relation of the new Boussinesq equations. When $h_s = 0$ and $\gamma = 0$, it reduces to the dispersion relation of the Boussinesq equations derived by Peregrine (1967). When $h_s = 0$, it reduces to that of the extended equations derived by Madsen et al. (1991).

To obtain the exact dispersion relation for porous beds, the linearized forms of Eqs. (17)–(25) for a horizontal bottom with constant porous thickness are analytically solved. The corresponding relation is (Gu and Wang, 1991; Cruz, 1994):

$$\omega^2 - gk\tanh kh = -iR\tanh kh_s(gk - \omega^2\tanh kh) \tag{96}$$

where R is the nondimensional parameter

$$R \equiv \frac{\lambda\omega}{\alpha_l} \tag{97}$$

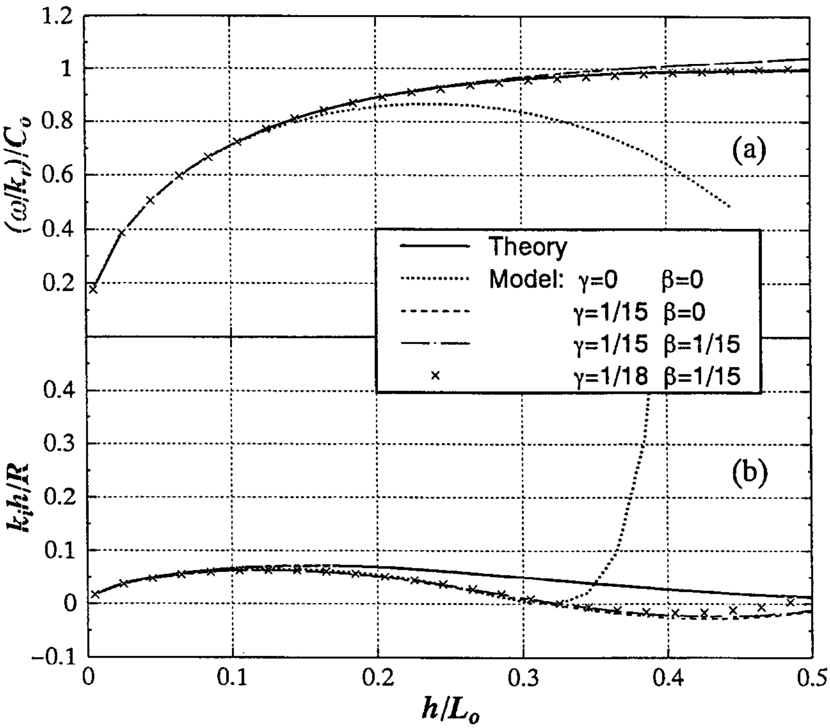

Fig. 2. Normalized phase celerities and porous damping rates. $R = 0.1$, $\lambda = 0.5$, $h_s/h = 0.2$.

The linear part α_l of α in Eq. (26) is commonly defined as (Sollitt and Cross, 1972):

$$\alpha_l \equiv \frac{\nu\lambda}{K} \tag{98}$$

where ν is the kinematic viscosity and K the intrinsic permeability. Hence, $R \equiv \omega k/\nu$ which is the nondimensional permeability. R is $O(10^{-6})$–$O(10^{-2})$ for sand and $O(10^{-1})$ at most, for gravel within the usual ranges of frequencies. For consistency with Eq. (96), we use $\alpha = \alpha_l$ and $c_r = 1.0$ in Eq. (95). For a given relative depth $h/L_0 \equiv \omega^2 h/(2\pi g)$, relative porous thickness h_s/h and R, kh can be solved from Eqs. (95) and (96). From Eq. (92),

$$\eta(x,t) = \alpha_0 e^{-k_i x} e^{i(k_r x - \omega t)} \tag{99}$$

so that the real part of the wave number governs the phase celerity component while the imaginary part corresponds to the spatial damping rate.

Figs. 2–4 show the solutions of Eqs. (95) and (96) as a function of h/L_0 for three values of the relative porous thickness h_s/h. The phase celerities shown in (a) are normalized by $C_0 = g/\omega$, while the damping rates shown in (b) are normalized by R/h. The dotted curves correspond to the basic Boussinesq equations. There is an upper bound of h/L_0 below which a solution to Eq. (96) exists. This bound decreases with increasing h_s/h. The original Boussinesq equations for impermeable beds are valid up

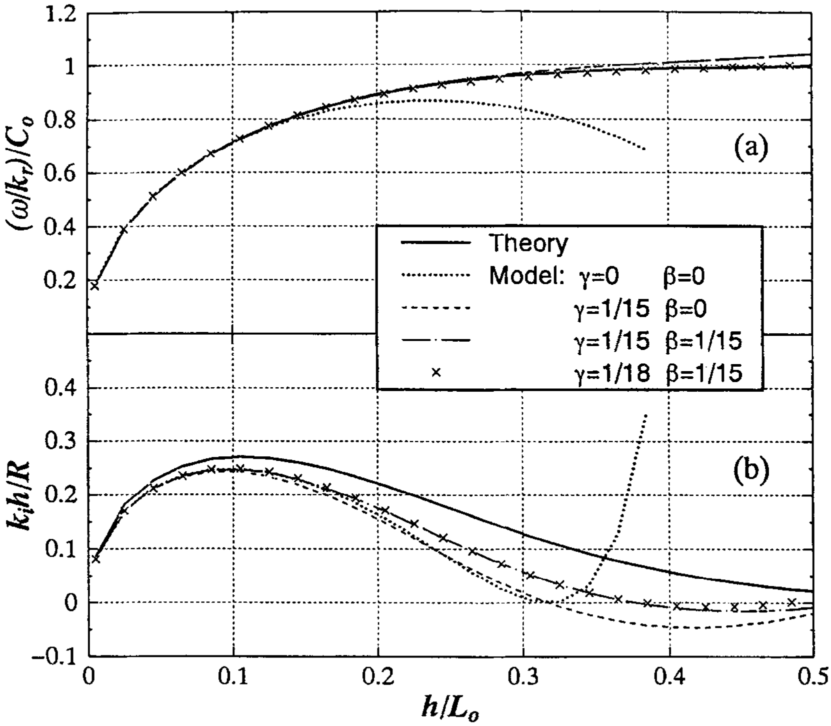

Fig. 3. Normalized phase celerities and porous damping rates. $R = 0.1$, $\lambda = 0.5$, $h_s/h = 1.0$.

to $h/L_0 = 0.22$ if a maximum relative error of 5% is allowed for celerity. In the presence of the porous layer, this bound becomes smaller if the damping rate is to be strictly satisfied. This more restrictive bound depends on h_s/h. The value $\gamma = 1/15$ which was determined by Madsen and Sorensen (1992) by satisfying both linear dispersion and shoaling gradient properties up to the deep water limit of $h/L_0 = 0.50$, corresponds to the dashed curve. Without extending the dispersion terms in the momentum equation for the porous layer, this value underestimates the damping property in intermediate waters especially for the thicker porous layers. Setting $\beta = 1/15$ improves the damping significantly. However, there is a noticeable increase of celerity in deeper waters. With $\gamma = 1/18$ and $\beta = 1/15$, the celerity is well satisfied up to the deep water limit and the amount of damping is significantly improved in deeper waters compared to the uncorrected equations.

There are alternative ways of extending the applicability bounds of the extended Boussinesq equations for porous beds. By selecting only certain terms in either or both momentum equations to use in obtaining the zero equations, we obtained various dispersion relations analogous to Eq. (95). Nine such alternative ways are included in Cruz (1994). One of these involves additional zero equations to those already shown here using the last dispersion terms in Eqs. (67) and (68). This improves the porous damping rate in deep water, that is, the damping rate is almost zero as h/L_0 approaches 1. However, β needs to be varied according to h_s/h and the resulting model equations

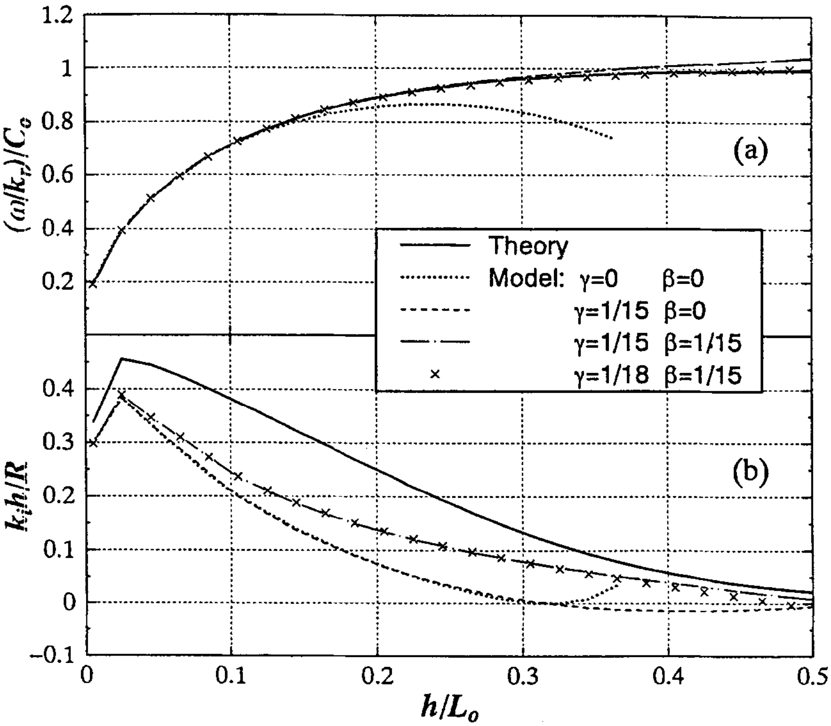

Fig. 4. Normalized phase celerities and porous damping rates. $R = 0.1$, $\lambda = 0.5$, $h_s/h = 5.0$.

are more elaborate. The extension scheme presented here is the optimum up to the specified bounds in h/L_0 and h_s/h and the most suitable for numerical implementation.

5. Applications of the Boussinesq equations for porous beds

5.1. Numerical computations

For brevity, the overbars in $\bar{u}$ and $\bar{u}_s$ are omitted. The numerical computations were carried out using finite differences. The solution utilizes an alternating-direction-implicit (ADI) algorithm that solves η, u and u_s then η, v and v_s in alternate fashion. The variables are defined on the staggered grid in Fig. 5a. The depths h, h_s are defined at the velocity grids. Spatial staggering is necessary for the discretization of the cross-derivative terms. Time staggering is needed to time-center the dominant gravity terms in the momentum equations; otherwise, artificial gravity would be created leading to eventual loss of water in the domain. η, $\boldsymbol{u}$ and $\boldsymbol{u}_s$ are split in time as shown in Fig. 5b. In the ADI algorithm, $\eta^{n+1/2}$, u^{n+1} and u_s^{n+1} are solved simultaneously in the x-sweep for all points, then η^{n+1}, $v^{n+3/2}$ and $v_s^{n+3/2}$ are solved together in the y-sweep. At each time level, ad-hoc values η^* or η^{**}, needed for the dispersion terms, are determined using an explicit discretization of the continuity equation. For concreteness,

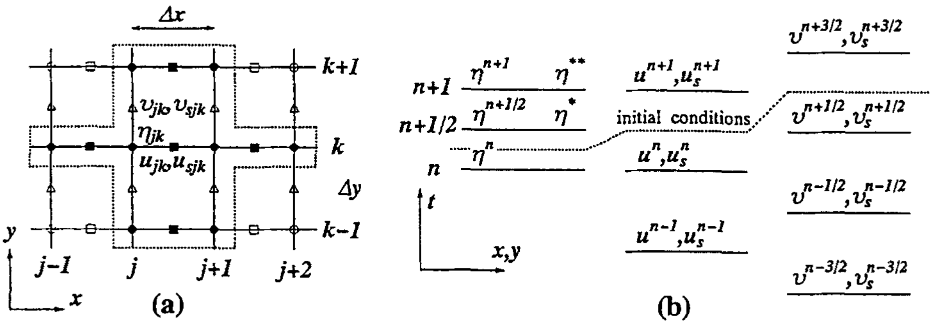

Fig. 5. Finite difference discretization. (a) Spatial grid for x-sweep. (b) Time-splitting method.

we illustrate a half-cycle of computations. Spatial differences are space-centered so only the time levels (superscripts) are shown. Continuity equation (70) is first discretized explicity for η

$$\frac{\eta_{jk}^{*}-\eta_{jk}^{n}}{\Delta t/2}+\left[(h+\eta^{n})u^{n}\right]_{x}+\left[(h+\eta)\frac{1}{2}\left(v^{n+1/2}+v_{s}^{n-1/2}\right)\right]_{y}+\left(h_{p}u_{s}^{n}\right)_{x}$$
$$+\left[h_{p}\frac{1}{2}\left(v_{s}^{n+1/2}+v_{s}^{n-1/2}\right)\right]_{y}=0 \tag{100}$$

where $h_{p}\equiv\lambda h_{s}$. After the above equation is solved for η^{*}, the calculation enters the ADI stage. Here, the continuity equation is discretized implicitly as

$$\frac{\eta_{jk}^{n+1/2}-\eta_{jk}^{n}}{\Delta t/2}+\left[(h+\eta^{*})\frac{1}{2}(u^{n+1}+u^{n})\right]_{x}$$
$$+\left[(h+\eta^{*})\frac{1}{2}(v^{n+1/2}+v^{n-1/2})\right]_{y}+\left[h_{p}\frac{1}{2}(u_{s}^{n+1}+u_{s}^{n})\right]_{x}$$
$$+\left[h_{p}\frac{1}{2}\left(v_{s}^{n+1/2}+v_{s}^{n-1/2}\right)\right]_{y}=0 \tag{101}$$

Momentum equation (84) is discretized as

$$\frac{u_{jk}^{n+1}-u_{jk}^{n}}{\Delta t}+(uu_{x}+vu_{y})^{n+1/2}+g\eta_{x}^{n+1/2}+\frac{h^{2}}{6}\left(\frac{u_{xx}^{n+1}-u_{xx}^{n}}{\Delta t}+v_{xyt}^{n+1/2}\right)$$
$$-\left(\frac{1}{2}+\gamma\right)h\left[\frac{(hu)_{xx}^{n+1}-(hu)_{xx}^{n}}{\Delta t}+(hv_{t})_{xy}^{n+1/2}\right]-\gamma gh\left[h\left(\eta_{xxx}^{*}+\eta_{yyx}^{*}\right)\right]$$
$$-\gamma gh\left[h_{x}\eta_{x}^{*}+h_{y}\eta_{y}^{*}\right]_{x}-\frac{1}{2}h\left\{\left[h_{p}\left(\frac{u_{s}^{n+1}-u_{s}^{n}}{\Delta t}\right)\right]_{xx}+\left(h_{p}v_{st}\right)_{xy}^{n+1/2}\right\}$$
$$+\epsilon\frac{1}{2}(u^{n+1}+u^{n})=0 \tag{102}$$

Momentum equation (88) is discretized as

$$
\begin{aligned}
& c_r\left(\frac{u_{s\,jk}^{n+1}-u_{s\,jk}^{n}}{\Delta t}\right)+c_r\left(u_s u_{s\,x}+v_s u_{s\,y}\right)^{n+1/2}+g\eta_x^{n+1/2}+\alpha\frac{1}{2}\left(u_s^{n+1}+u_s^{n}\right)\\
& -\frac{1}{3}c_r h_s^2\left(\frac{u_{s\,xx}^{n+1}-u_{s\,xx}^{n}}{\Delta t}+v_{s\,xyt}^{n+1/2}\right)-\frac{1}{2}c_r h_s\left\{\left[h_{bx}\left(\frac{u_s^{n+1}-u_s^{n}}{\Delta t}\right)\right]_x\right.\\
& \left.+\left(h_{by}v_{st}\right)_x^{n+1/2}\right\}+\frac{1}{2}c_r h_s\left(h_x-h_{s\,x}\right)\left[\left(\frac{u_{s\,x}^{n+1}-u_{s\,x}^{n}}{\Delta t}\right)+v_{s\,yt}^{n+1/2}\right]\\
& +c_r h_x\left[h_{bx}\left(\frac{u_s^{n+1}-u_s^{n}}{\Delta t}\right)+\left(h_{by}v_{st}\right)^{n+1/2}\right]\\
& -\frac{1}{3}\alpha h_s^2\left[\frac{1}{2}\left(u_{s\,xx}^{n+1}+u_{s\,xx}^{n}\right)+v_{s\,xy}^{n+1/2}\right]-\frac{1}{2}\alpha h_s\left[h_{bx}\frac{1}{2}\left(u_s^{n+1}+u_s^{n}\right)_x\right.\\
& \left.+\left(h_{by}v_s\right)_x^{n+1/2}\right]+\frac{1}{2}\alpha h_s\left(h_x-h_{s\,x}\right)\left[\frac{1}{2}\left(u_{s\,x}^{n+1}+u_{s^n x}\right)+v_{s\,y}^{n+1/2}\right]\\
& +\alpha h_x\left[h_{bx}\frac{1}{2}\left(u_s^{n+1}+u_s^{n}\right)+\left(h_{by}v_s\right)^{n+1/2}\right]\\
& -\frac{1}{2}\left\{\left[h^2\left(\frac{u^{n+1}-u^{n}}{\Delta t}\right)\right]_{xx}+\left(h^2 v_t\right)_{xy}^{n+1/2}\right\}\\
& -(1+\beta)\left\{\left[h\left(h_p\frac{u_s^{n+1}-u_s^{n}}{\Delta t}\right)_x\right]_x+\left[h\left(h_p v_{st}\right)_y\right]_x^{n+/2}\right\}\\
& -\frac{\beta g}{c_r}\left\{h\left[\left(h_p\eta_x^*\right)_x+\left(h_p\eta_y^*\right)_y\right]\right\}_x-\frac{\beta\alpha}{c_r}\left\{\left[h\left(h_p\frac{1}{2}\left(u_s^{n+1/2}+u_s^{n}\right)\right)_x\right]_x\right.\\
& \left.+\left[h\left(h_p v_s\right)_y\right]_x^{n+1/2}\right\}=0
\end{aligned}
\tag{103}
$$

The last term in Eq. (102) is the boundary damping term in the absorption region needed to enforce the open boundary condition.

The nonlinear convection terms are discretized so that they are space-centered at (j,k) and time-centered at $n+1/2$; for example,

$$
\begin{aligned}
(uu_x)^{n+1/2} &\equiv \frac{1}{2}\left(u^2\right)_x^{n+1/2}\\
&= \frac{\frac{1}{2}\left(u_{jk}^{n+1}+u_{j+1,k}^{n+1}\right)\cdot\frac{1}{2}\left(u_{jk}^{n}+u_{j+1,k}^{n}\right)-\frac{1}{2}\left(u_{j-1,k}^{n+1}+u_{jk}^{n+1}\right)\cdot\frac{1}{2}\left(u_{j-1,k}^{n}+u_{jk}^{n}\right)}{2\Delta x}
\end{aligned}
\tag{104}
$$

The nonlinear advection terms are discretized using the angular derivative method (Kowalik and Murty, 1993, pp. 50–52). In a single equation, this can be generalized as

$$(vu_y)^{n+1/2} = \frac{\bar{v}}{2\Delta y}\left[(f_1-f_2)\left(u_{jk}^{n+1}-u_{jk}^{n}\right)+f_1u_{j,k+1}^{n}+f_2u_{j,k+1}^{n+1}-\left(f_1u_{j,k-1}^{n+1}+f_2u_{j,k-1}^{n}\right)\right] \tag{105}$$

$$\bar{v}=\frac{1}{4}\left(v_{j,k-1}^{n+1/2}+v_{j+1,k-1}^{n+1/2}+v_{jk}^{n+1/2}+v_{j+1,k}^{n+1/2}\right) \tag{106}$$

$f_1=1$ $\quad f_2=0$ $\quad$ increasing y
$f_1=0$ $\quad f_2=1$ $\quad$ decreasing y

The cross-derivative dispersion terms in the momentum equations must be defined at time level $n+1/2$. We employed an extrapolation method similar to Madsen and Sorensen (1992) using values at the three most recent time levels. For example (see Fig. 5b):

$$(hv_t)_{xy}^{n+1/2}=\frac{3}{2}(hv_t)_{xy}^{n}-\frac{1}{2}(hv_t)_{xy}^{n-1} = \frac{3(hv)_{xy}^{n+1/2}-4(hv)_{xy}^{n-1/2}+(hv)_{xy}^{n-3/2}}{2\Delta t} \tag{107}$$

Similar discretizations are employed for terms like $v_{txy}^{n+1/2}$, $(h_p v_{st})_{xy}^{n+1/2}$, etc.

5.2. Damped wave propagation on uniform porous bed

The basic properties of the new Boussinesq equations are illustrated by testing for one-dimensional propagation of a plane wave. The computational domain is shown in Fig. 6c. Regular wave trains enter from the left and exit at the right where a sponge layer is placed to enforce the open boundary condition. The boundary damping represented by $\epsilon(x)$ in Eq. (102) is distributed parabolically for incident waves with $h/L_0>0.10$ and linearly for $h/L_0<0.10$. The optimum values of the maximum damping coefficient for a given damping width have been determined from graphs in Cruz and Isobe (1994) for regular waves, assuming no porous layer. At the left boundary, $u(t)$ and the spatial gradient of η, evaluated from an arbitrary-order Stokes wave theory (Horikawa, 1988, pp. 26–30) and $u_s=0$ were prescribed. At the other end, Sommerfeld radiation conditions for η and u with the celerity $\sqrt{gh}$ and $u_s=0$ were enforced. The nonlinear terms in the model equations, except for the α_2 component of the resistance equation, were all included. In the following results, the relative porous thickness h_s/h was set at 1.0 and the porosity λ is 0.50. We verify the new Boussinesq equations by varying the incident wave conditions and the porous medium property R.

In Fig. 6, a linear wave with intermediate dispersivity and small permeability is incident at $x=0$. As shown by the wave profile in Fig. 6b, the model equations agree

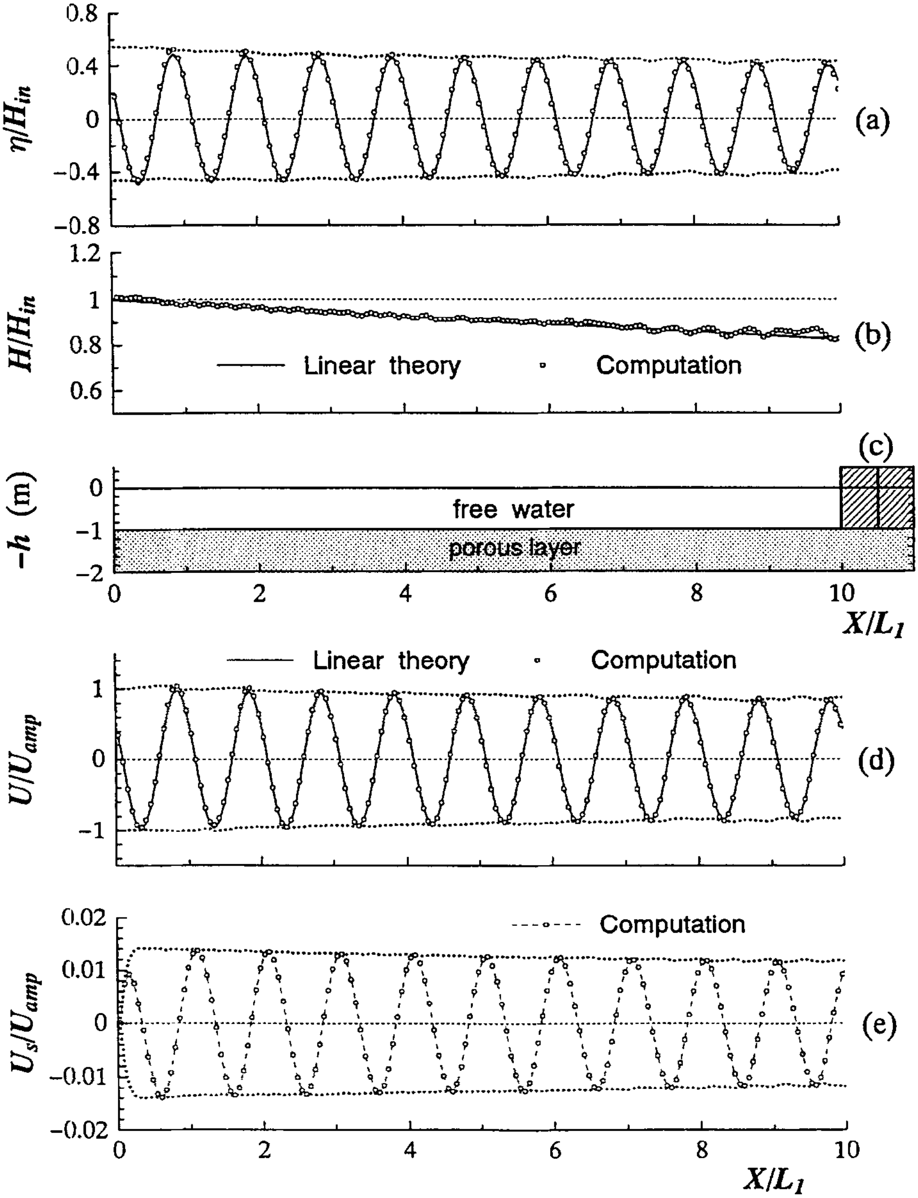

Fig. 6. Wave propagation on uniform porous bed. $h_s / h = 1.0$, $R = 0.1$, $H_{in} / h = 0.02$, $h / L_0 = 0.10$.

almost completely with theory. The amount of porous damping, indicated by the normalized wave height distribution in Fig. 6b, is also well reproduced, disregarding the persistent oscillation caused by the expedient use of $u_s = 0$ at the boundaries. The velocity profiles are also shown and a comparison with theory is indicated for $u(t)$.

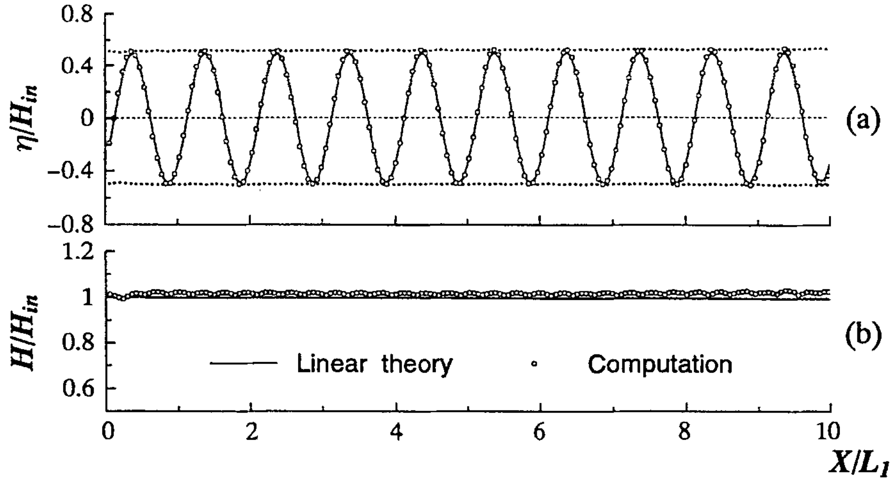

Fig. 7. Wave propagation on uniform porous bed. $h_s/h = 1.0$, $R = 0.1$, $H_{in}/h = 0.02$, $h/L_0 = 0.50$.

These are normalized by $U_{amp} \equiv CH_{in}/2h$ where C is the linear celerity and H_{in} is the incident wave height. The profiles suggest that $u_s = 0$ is not realistic when the porous layer extends to the ends. These profiles also show that the seepage velocities are small compared to the free water velocities. However, u_s is partially off-phase with u, indicating a friction-type damping action that is compatible with the use of $\alpha = \alpha_l$ in the linear case.

In Fig. 7, the deep water limit $h/L_0 = 0.50$ is used. The incident wave travels at the free wave celerity without being damped. Since the particle velocities below the interface do not penetrate the porous layer, the seepage velocities (not shown) are negligibly small, precluding wave energy dissipation through the porous medium.

In Fig. 8, the incident wave is a second-order Stokes wave with a nonlinearity index one order of magnitude higher than that in Fig. 6. Fig. 8b shows that for intermediate dispersivity, the damping rate is unchanged although the vertical asymmetry in the wave profile is already prominent. The seepage velocities remain small relative to the velocities in the free water. In Fig. 9, the porous medium is more permeable while the incident wave nonlinearity is very small. The absolute amount of damping per wavelength is considerably increased. There is excellent agreement of wave and velocity profiles between computation and theory. The computed seepage velocities are increased by one order of magnitude that resulted in the decayed wave heights shown.

5.3. Wave transformation on plane porous slope

The new Boussinesq equations have been used to simulate the damped shoaling wave transformation on a plane porous slope. Experiments were conducted in a 0.30 × 0.20 × 11.0 m wave flume at the University of Tokyo. The set-up is shown in Fig. 10b. The physical model of the triangular porous bar has side slopes of 1 : 20 and 1 : 6.67 and was built from 0.67 cm natural gravel. Measured porosity was 0.44. The maximum h_s/h is

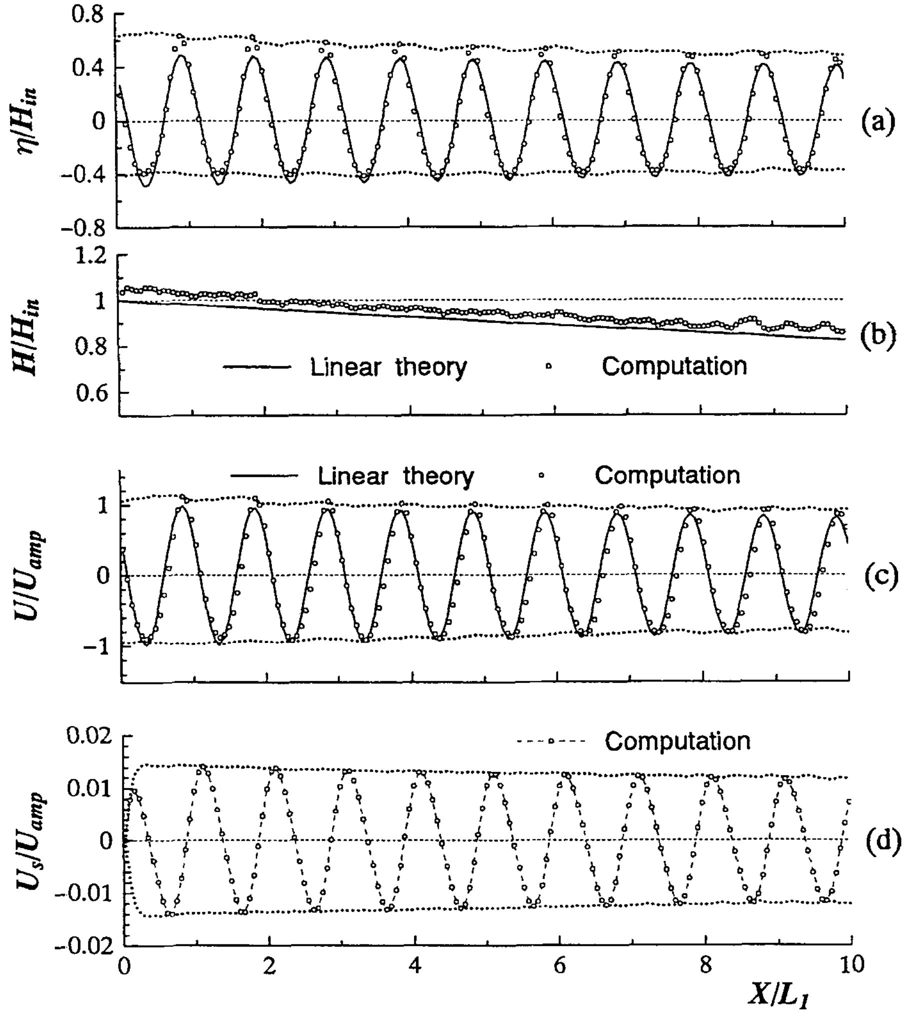

Fig. 8. Wave propagation on uniform porous bed. $h_s/h = 1.0$, $R = 0.1$, $H_{in}/h = 0.20$, $h/L_0 = 0.10$.

2.9 at the apex of the bar. Eight capacitance-type wave gauges were placed to record the surface displacements and two gauges (not shown) were used to resolve the incident and reflected waves using the two-point method of Goda and Suzuki (1976). In the experiment, incident waves were generated by a flap-type wave paddle at $x = 0$ and absorbed at the other end by a meshed screen. The following resistance equation of Sollitt and Cross (1972) is used for α_1 and α_2 in Eq. (26):

$$\alpha \equiv \frac{\nu\lambda}{K} + \frac{C_f \lambda^2}{\sqrt{K}}|u_s| \tag{108}$$

where ν is the kinematic viscosity and C_f the turbulent friction coefficient. The values

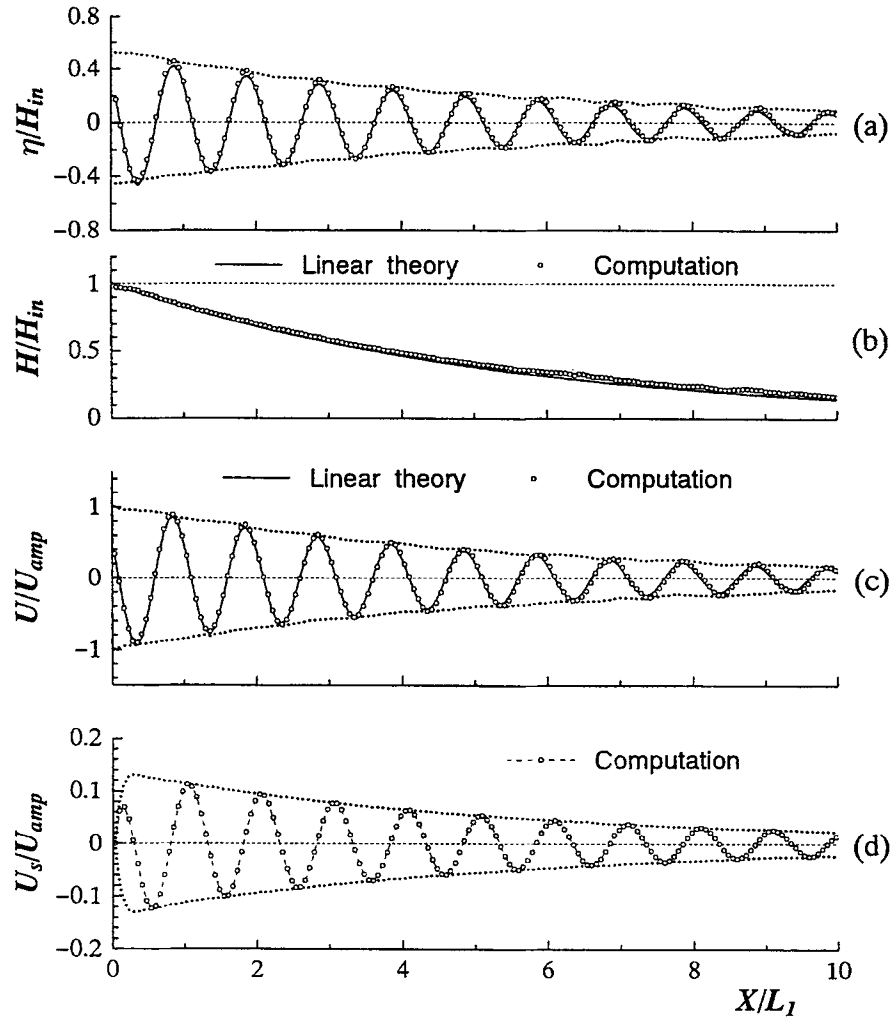

Fig. 9. Wave propagation on uniform porous bed. $h_s/h = 1.0$, $R = 1.0$, $H_{in}/h = 0.02$, $h/L_0 = 0.10$.

used are: $\nu = 8.9 \times 10^{-3}$ cm^2/s (at 25°C), $c_m = 0$, $K = 2.5 \times 10^{-4}$ cm^2 and $C_f = 0.40$. K and C_f were extrapolated from the tabulated data of Sollitt and Cross (1972) using the measured gravel size. Computations were carried out under the same boundary conditions as in the preceding section, except that now the condition $u_s = 0$ models the actual conditions at the ends of the domain. Results were obtained after the profiles have steadied.

Results for three cases are shown in Figs. 10–12. Fig. 10 shows the measured and computed wave heights and profiles for an incident wave with small nonlinearity and intermediate dispersivity. In order to verify the phase property, the reference time $t = 0$ for all stations was taken by lapping the measured and computed profiles at Station 1.

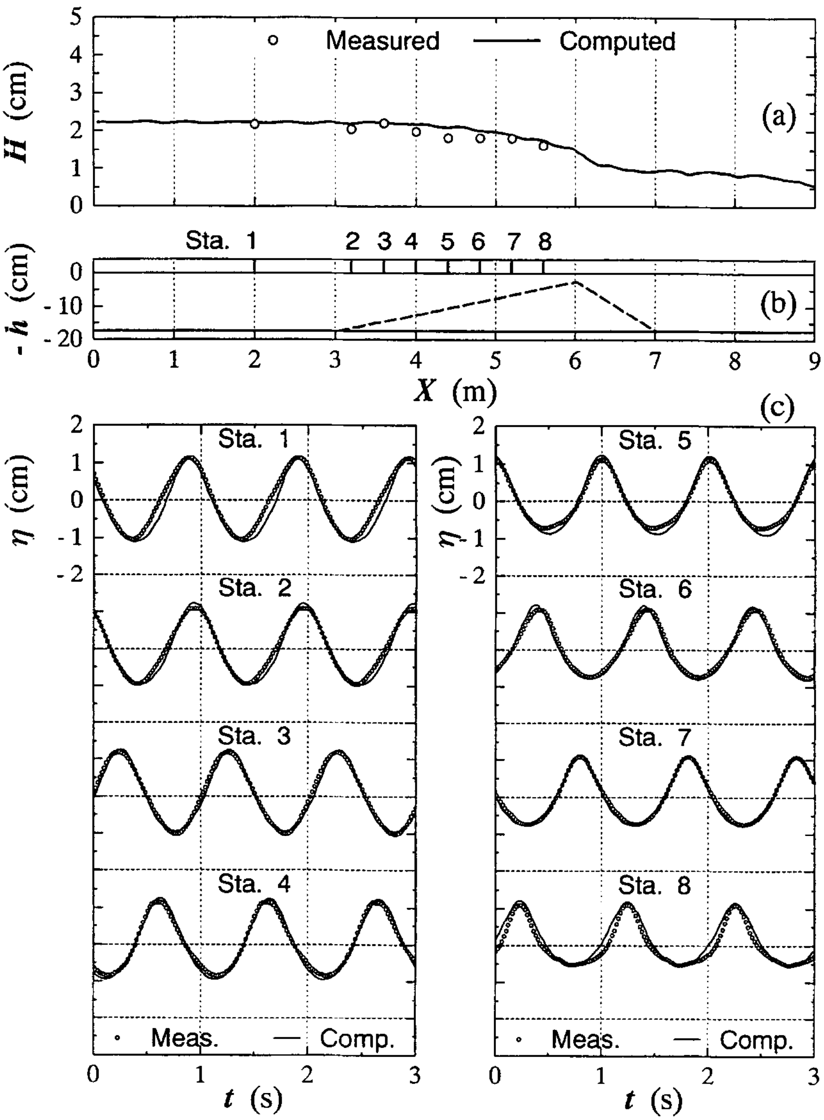

Fig. 10. Wave transformation on plane porous slope. $H_{in} = 2.2$ cm, $T = 1.02$ s, $H_{in} = 0.125$, $h/L_0 = 0.108$.

The general trend of the damped wave height is predicted quite well by the model. The phase relation between the stations is well reproduced as the dispersivity of the incident wave is within the applicability bound of the basic equations.

In Fig. 11, the incident wave nonlinearity is roughly doubled so that measurements indicated breaking around $x = 5.8$ m. In the calculation, the rear face of the bar was moved seaward as shown in (b) so that the minimum depth h at the apex allowed the wave to pass without breaking. The measured and computed profiles agree well at all

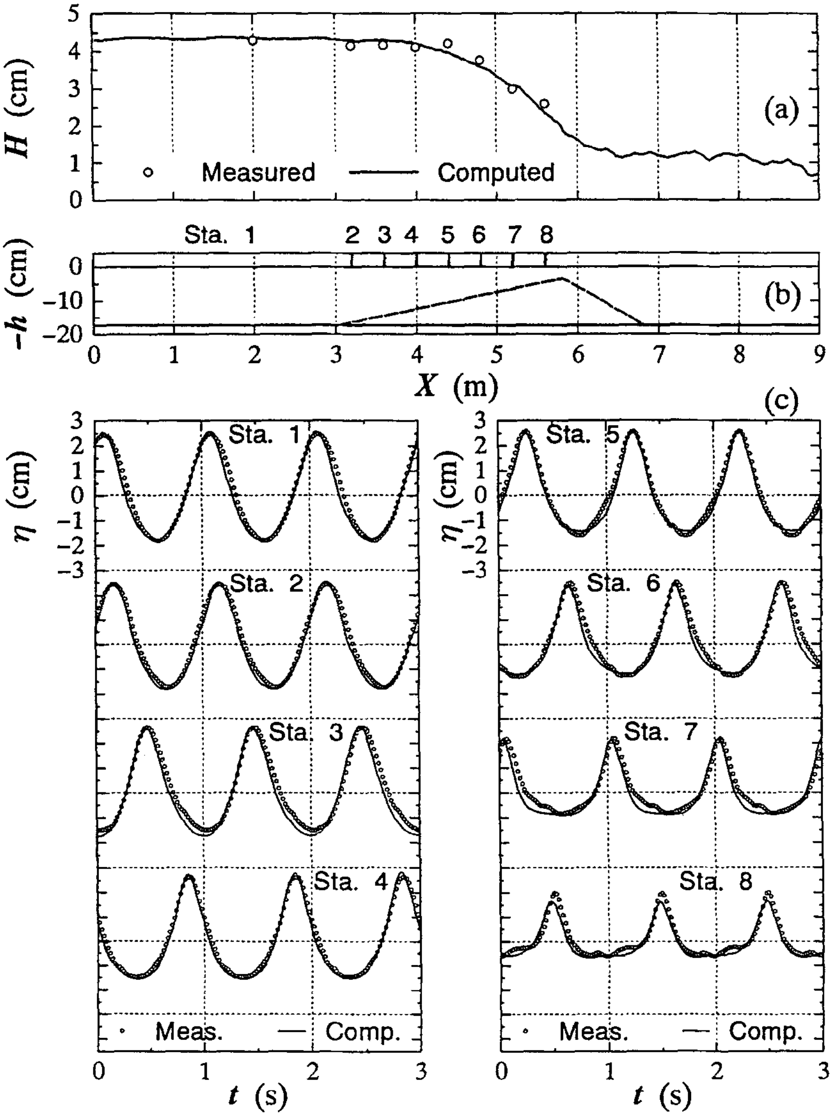

Fig. 11. Wave transformation on plane porous slope. $H_{in} = 4.3$ cm, $T = 1.00$ s, $H_{in}/h = 0.246$, $h/L_0 = 0.115$.

stations except the last two which are nearest the breaking location. Measurements show that energy in the higher frequencies is released by the breaking process which seemed to have slowed down the primary wave. The wave height distribution is predicted well especially the rapid dissipation measured at stations on thicker porous layer, although this appears to be at the expense of underestimation of the initial shoaling effect.

In Fig. 12, the incident dispersivity is small and the nonlinearity is high. Measurements at the resolution gauges indicated the presence of significant amplitude in the

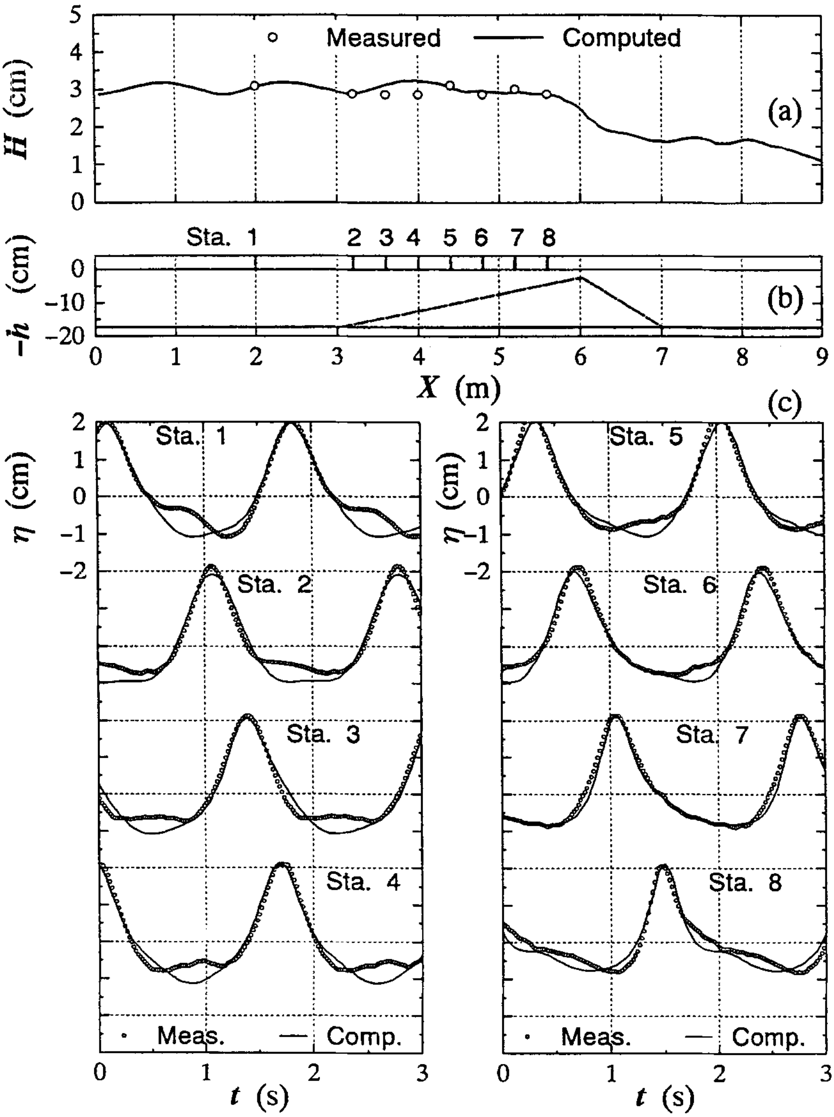

Fig. 12. Wave transformation on plane porous slope. $H_{in} = 3.1$ cm, $T = 1.72$ s, $H_{in}/h = 0.188$, $h/L_0 = 0.038$.

second harmonic (see profile at Station 1) caused by the nonlinear boundary conditions at the reflective wave paddle which were not simulated in the computations. This harmontic persists up to a distance from the toe, corrupting the profiles as far as Station 5. From there, the damping effect of the porous bar dominates and efficiently damps the higher harmonic out of the domain. Wave heights based on envelopes of measured profiles indicate that shoaling commences only after Station 4 while computation indicates that it began early on. The difference is explained by the fact that the shoaling and damping elements in the model equations operate on different. freqnencies with different degrees and the existence of the higher harmonic seems to complicate which element is dominant in the initial stage. The distribution of wave height is still predicted quite well by the model.

5.4. Wave transformation around submerged porous breakwater with an opening

A practical application of the Boussinesq equations for porous beds is the simulation of the wave field around submerged porous breakwaters. To test the applicability of the equations, we conducted experiments on a $2.9 \times 6.0 \times 0.25$ m wave basin at the University of Tokyo. The breakwater model consists of two 0.84 m wide trapezoidal mounds built from 0.67 cm gravel symmetrically disposed along the centerline. The bathymetry, normalized by the uniform depth to bottom, is shown in Fig. 13. The mound sides were sloped at 1:2 all around allowing a maximum opening of 0.74 m at the crown. The depth of water on the horizontal bottom was 14 cm and the porous thickness at the crown was 8 cm. Regular waves were generated by a flap-type paddle at the left end and absorbed by a meshed screen at the other end. The hydraulic properties of the porous medium are as they were in the preceding wave flume experiments. The sides of the basin were solid vertical walls where waves are completely reflected. Wave profiles were taken at 136 points in the symmetrical half around the lower mound. By assuming that these profiles are duplicated in the other half, the wave height distribution in Fig. 14a, normalized by the incident wave height H_{in}, was obtained for one non-breaking case. To resolve the incident and reflected waves, the method of Goda and Suzuki (1976) was used, aware of the fact that multi-directional waves existed everywhere in the basin.

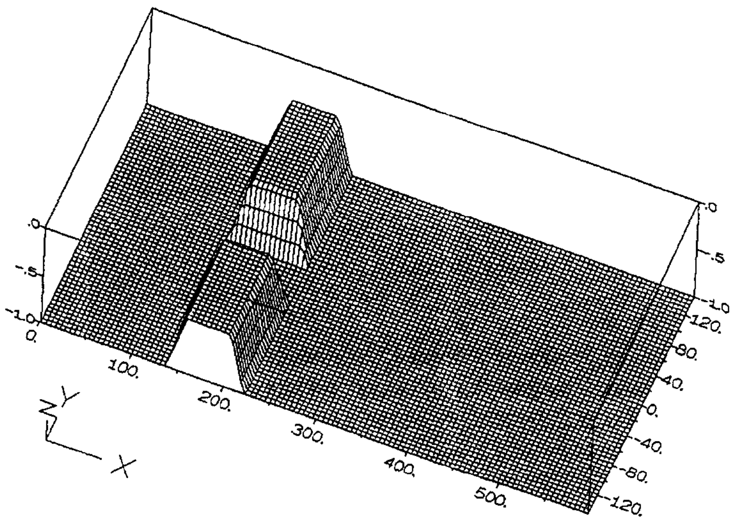

Fig. 13. Submerged porous breakwater bathymetry.

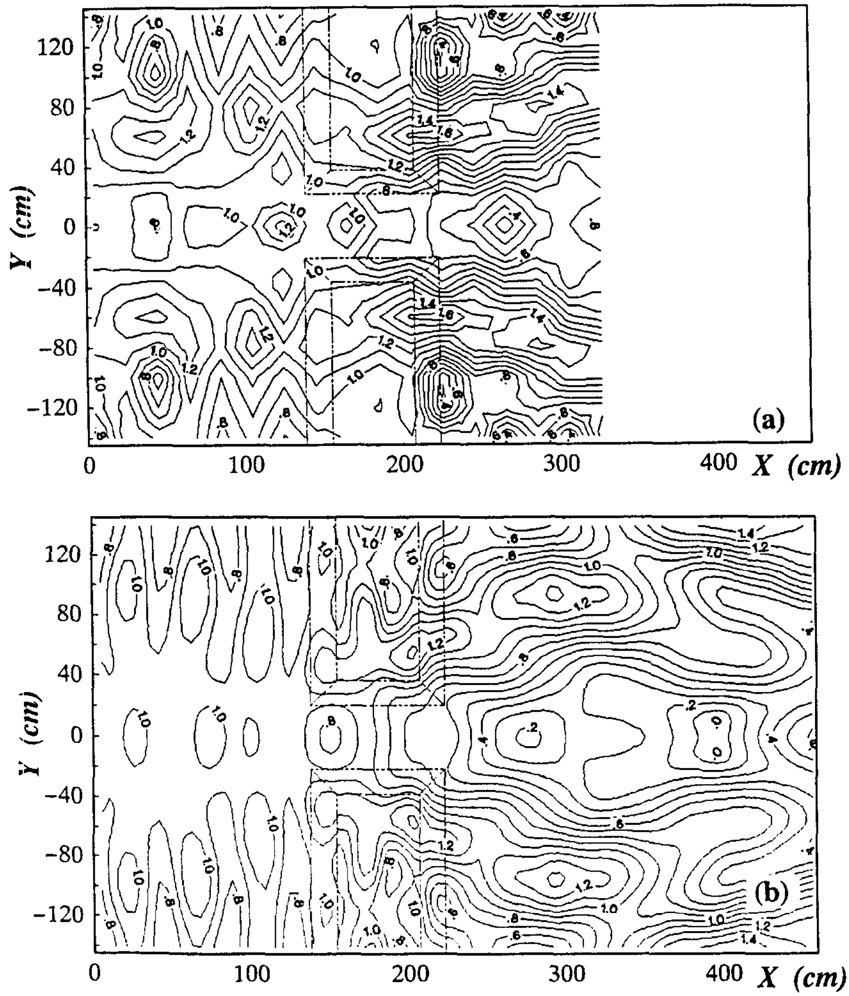

Fig. 14. H/H_{in} distribution. (a) Experiments. (b) Computation.

Absorption of waves at the absorber end of the basin was implemented by attaching a transverse strip of energy-absorbing region beginning at $x = 460$. The properties of the absorber are: relative damping width $F/h_b = 10$, maximum damping coefficient $\theta = 0.40$, and damping distribution: linear. For a maximum reflection of 3%, the rough range of absorbable frequencies is $h/L_0 = 0.04$–1.0 which is sufficient even when wave decomposition occurs at the lee. Preliminary computations were carried out assuming that all sea-bound waves were completely radiated out of the domain.

Fig. 14b shows the computed normalized wave heights for one trial run where the incident wave height and period were 1.48 cm and 0.82 s, respectively. The computed seaward wave field indicates the coexistence of oblique waves scattered by the opening, normal waves reflected by the mounds, and multi-directional outgoing waves reflected

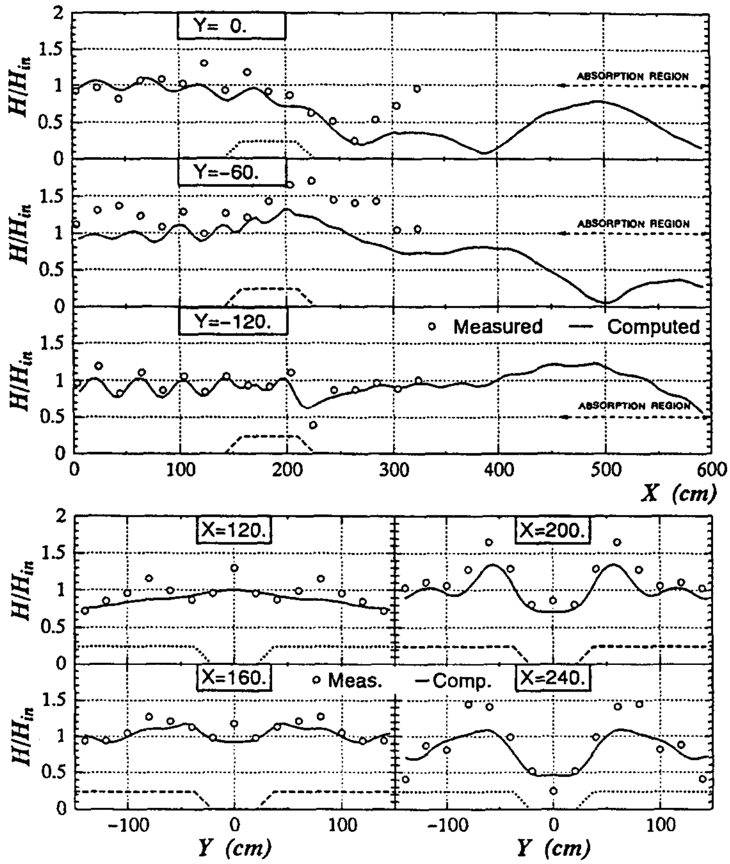

Fig. 15. Sectional distributions of H/H_{in}.

by the side walls. On the shallow crowns, the combined effects of mound-induced refraction, diffraction, depth-reflection, shoaling and porous damping, and wall-induced multi-reflection have resulted in the complicated wave pattern shown. The shoreward wave field is dominated by effects of diffraction and refraction by the mound and reflection from the walls. When compared with the measured wave height distribution, the computed result reproduces the gross features of the wave field quite well. The spatial distributions of wave heights along longitudinal and transverse sections are shown in Fig. 15.

The difference in the computed and measured wave fields, particularly in the seaward region, is due to the neglect of the actual reflective condition at the wave generator that forced the sea-bound waves to return into the interior without substantial loss of energy. To properly simulate this condition, we have used an interior wave generation method together with an absorption region of minimal damping to induce the waves to propagate back into the domain. The quantitative improvements in the wave fields (not shown here), especially at the seaward region, are considerable. Results and details that discuss this boundary treatment will be reported in a separate paper.

6. Conclusions

The main conclusions from this study are summarized as follows:

A set of vertically-integrated time-dependent equations of continuity and momentum is derived to model the horizontally two-dimensional transformation of waves over porous beds on uneven bottoms. The equations incorporate the leading orders of wave nonlinearity and dispersivity and are applicable to weakly nonlinear, weakly dispersive waves. The form of the resistance equation of the porous medium has been generalized to include possible application to flows of high turbulence in field conditions.

The applicability bounds of the basic Boussinesq equations for porous beds have been extended by improving the linear dispersion and spatial damping properties up to the deep water limit. By adding dispersion terms obtained from the lowest-order momentum equations and determining the two extension factors γ and β thereby introduced such that the linearized equations significantly match the dispersion relation and damping rates of the linear theory for porous beds, the new Boussinesq equations can be used with $\gamma = 1/18$, $\beta = 1/15$ up to a relative depth $h/L_0 = 0.50$ and relative porous thickness $h_s/h = 5$.

A numerical procedure for the two-dimensional implementation is discussed. The basic properties of the model are verified by performing computations for wave propagation on horizontal bottom of uniform thickness and comparing the results with theory. Under compatible conditions, the agreement is very good. The model is also tested for the simulation of damped shoaling wave transformation on plane porous slope and of the wave field around a submerged porous breakwater with an opening. The good agreement with the wave heights and profiles of the experiments verifies the applicability of the model.

References

Cruz, E.C., 1994. Modelling of nonlinear, dispersive wave transformation around submerged porous breakwaters. Doctoral dissertation. Dept. Civil Eng., Univ. Tokyo, 133 pp.

Cruz, E.C. and Isobe, M., 1994. Numerical wave absorbers for short and long wave modelling. In: Proc. Int. Symp. on Waves — Phys. and Num. Modelling, Univ. British Columbia, Vol. 2, pp. 992–1001.

Cruz, E.C., Isobe, M. and Watanabe, A., 1992. Nonlinear wave transformation over a submerged permeable breakwater. In: Proc. 23rd Int. Conf. Coastal Eng., Venice. ASCE, pp. 1101–1114.

Goda, Y. and Suzuki, Y., 1976. Estimation of incident and reflected waves in random wave experiments. In: Proc. 15th Int. Conf. Coastal Eng., Honolulu, HI. ASCE, pp. 828–845.

Gu, Z. and Wang, H., 1991. Gravity waves over porous bottoms. Coastal Eng., 15: 497–524.

Horikawa, K. (Editor), 1988. Nearshore Dynamics and Coastal Processes. Univ. Tokyo Press, 522 pp.

Isobe, M. and Kraus, N.C., 1983a. Derivation of a third-order Stokes wave theory. Technical Report No. 83-1. Hydraulics Lab., Dept. Civil Eng., Yokohama National Univ., 37 pp.

Isobe, M. and Kraus, N.C., 1983b. Derivation of a second-order cnoidal wave theory. Technical Report No. 83-2. Hydraulics Lab., Dept. Civil Eng., Yokohama National Univ., 43 pp.

Isobe, M., Shiba, K., Cruz, E.C. and Watanabe, A., 1991. On the nonlinear deformation of waves due to submerged permeable breakwaters (in Japanese). Proc. Coastal Eng. JSCE, 38(1): 551–555.

Kioka, W., Kai, H. and Hiraoka, S., 1994. Nonlinear shallow water waves over a porous structure (in Japanese). Proc. Coastal Eng. JSCE, 41(1): 711–715.

Kowalik, Z. and Murty, T.S., 1993. Numerical Modelling of Ocean Dynamics. World Scientific, Singapore, 481 pp.

Madsen, P.A. and Sorensen, O.R., 1992. A new form of the Boussinesq equations with improved linear dispersion characteristics. Part 2: a slowly-varying bathymetry. Coastal Eng., 18: 183–205.

Madsen, I.A., Murray, R. and Sorensen, O.R., 1991. A new form of the Boussinesq eqnations with improved linear dispersion characteristics. Coastal Eng., 15: 371–388.

Mei, C.C., 1989. The Applied Dynamics of Ocean Surface Waves. World Scientific, Singapore, 740 pp.

Nwogu, O., 1993. Alternate form of Boussinesq equations for nearshore wave propagation. J. Waterw. Port Coastal Ocean Eng. ASCE, 119(6): 618–638.

Peregrine, D.H., 1967. Long waves on beaches. J. Fluid Mech., 27(4): 815–827.

Rojanakamthorn, S., Isobe, M. and Watanabe, A., 1990. Modeling of wave transformation on submerged breakwater. In: Proc. 22nd Int. Conf. Coastal Eng., Delft, 1990. ASCE, pp. 1060–1073.

Sawaragi, T. and Deguchi, I., 1992. Waves on permeable layers. In: Proc. 23rd Int. Conf. Coastal Eng., Venice. ASCE, pp. 1531–1544.

Sollitt, C.K. and Cross, R.H., 1972. Wave transmission through permeable breakwater. In: Proc. 13th Int. Conf. Coastal Eng., Vancouver, B.C. ASCE, pp. 1827–1846.

Witting, J.U., 1984. A unified model for the evolution of nonlinear water waves. J. Comp. Phys., 56: 203–236.